Check for updates

ADVANCED FUNCTIONAL MATERIALS
www.afm-journal.de

Unique Performance Considerations for Printable Organic Semiconductor and Perovskite Radiation Detectors: Toward Consensus on Best Practice Evaluation

Jessie A. Posar, Matthew Large, Andrea Ciavatti, Laura Basiricò, Beatrice Fraboni, Paul J. Sellin, Attila J. Mozer, Marco Petasecca, and Matthew J. Griffith**

Metal halide perovskites and organic semiconductors have attracted intense interest for ionizing radiation detection due to their advantages of strong attenuation, low leakage currents, synthetic versatility, and simple device manufacturing. These materials present opportunities to develop devices for safer medical imaging and dosimetry, sensing, shielding technologies for space exploration, and improved non-invasive analysis for security, product inspection, and nuclear safety. However, there is currently a glaring lack of standard approaches for testing and reporting the performance of novel organic semiconductor and perovskite-based materials and device architectures for radiation detection. This absence of standardization has resulted in a recent exponential increase in publications that lack consistency in both the experimental procedures used for characterization and the interpretation of performance parameters reported. In this Perspective, the major photophysics of organic semiconductors and perovskite materials under high-energy radiation are summarized, with limitations in evaluating radiation detection performance using metrics designed for highly crystalline inorganic technologies discussed. Finally, key metrics and experimental details that are suggested for reporting in publications to improve reproducibility and enable large data set analysis are identified, noting these procedures are not intended as an exhaustive or definitive list, but rather as a milestone toward enabling improved standardization.

1. Introduction

The use of ionizing radiation has experienced rapid growth in a wide range of applications, including fundamental materials characterization, medical diagnostics and treatment, space exploration, nuclear energy, security inspection, and wearable health monitoring.[1–4] Quantitative evaluation of radiation intensity is critical to not only extract useful technical information in scientific applications, but also to ensure safe use and implementation of emerging radiation technologies. Historically, crystalline inorganic semiconductors such as silicon[5,6] and cadmium telluride[7,8] have dominated the radiation detection research field, however, these materials exhibit limitations with processing into large-area pixelated detector matrices, an inability to create flexible devices that conform to the curved surfaces of the human body, and are expensive to manufacture at electronics-grade purity.[9] Demand for novel radiation detecting materials that

J. A. Posar, M. Large
Centre for Medical Radiation Physics
University of Wollongong
Wollongong, NSW 2522, Australia
E-mail: j.posar@uow.edu.au

J. A. Posar, M. J. Griffith
School of Aeronautical
Mechanical and Mechatronic Engineering
University of Sydney
Camperdown, NSW 2506, Australia
E-mail: matthew.griffith@unisa.edu.au

A. Ciavatti, L. Basiricò, B. Fraboni, M. Petasecca
Department of Physics and Astronomy
University of Bologna
Viale Berti Pichat 6/2, Bologna 40127, Italy

P. J. Sellin
Department of Physics
University of Surrey
Guildford, Surrey GU2 7XH, UK

A. J. Mozer
Intelligent Polymer Research Institute
Innovation Campus
Squires Way, North Wollongong, NSW 2500, Australia

M. J. Griffith
Future Industries Institute
University of South Australia
Mawson Lakes, SA 5095, Australia

The ORCID identification number(s) for the author(s) of this article can be found under https://doi.org/10.1002/adfm.202423521

© 2025 The Author(s). Advanced Functional Materials published by Wiley-VCH GmbH. This is an open access article under the terms of the Creative Commons Attribution License, which permits use, distribution and reproduction in any medium, provided the original work is properly cited.

DOI: 10.1002/adfm.202423521

16163028, 2026, 21, Downloaded from https://advanced.onlinelibrary.wiley.com/doi/10.1002/adfm.202423521 by Adelaide University, Wiley Online Library on [30/09/2026]. See the Terms and Conditions (https://onlinelibrary.wiley.com/terms-and-conditions) on Wiley Online Library for rules of use; OA articles are governed by the applicable Creative Commons License

can address these limitations has created strong interest in printable semiconductors, where the unique properties of organic polymers and metal halide perovskites have been shown to excel at various aspects of radiation detection.[10–13] Both organic semiconductors and perovskites provide low-cost synthesis and low-temperature solution-processability,[14] which enables a pathway toward thin and flexible devices that can be fabricated via low-cost roll-to-roll manufacturing for rapid industrial translation.[15–18]

Metal halide perovskites are characterized by an ABX_3 stoichiometry, where A is a monovalent cation (e.g., Cs^+ or $CH_3NH_3^+$), B is a metal (e.g., Pb^{2+} or Bi^{2+}) and X a monovalent anion (typically I^-, Br^-, or Cl^-, but pseudo-halide anions have also been employed).[19–21] Perovskites typically exhibit highly crystalline structures with excellent optoelectronic properties (e.g., high mobility, long carrier drift lengths) and high atomic number (Z) atoms (e.g., Pb, I, Br), providing a high attenuation coefficient for ionizing radiation.[22] In contrast, organic semiconductors are typically disordered materials with significant amorphous structural domains that maximize optoelectronic properties through nanoscale device engineering.[23] Their predominantly carbon-based composition results in fewer direct interactions with ionizing radiation, which can be improved by using thick active layers (≈10 µm) or by adding high Z materials for hybrid organic-inorganic active layer materials or substrates.[24,25] However, pristine organic semiconducting thin films employed in photodiode detectors (≈100 nm) are almost entirely transparent to ionizing radiation, making them an ideal technology for radiation dosimeters that do not perturb the incident beam.[26,27]

Despite strong interest in these emerging detector technologies, many of the characterization protocols for determining the performance of ionizing radiation materials were designed for traditional inorganic materials. There remains a lack of uniformity and clear standards for best practice characterization procedures that capture the performance of organic semiconductors and perovskite materials to a level that is transferable across technologies, device architectures and laboratories.[28] The material properties, device photo physics, and detector architectures that apply to perovskites and organic semiconductors are fundamentally different to inorganic materials and devices.[29,30] Thus, use of historical characterization metrics designed for crystalline inorganic photoconductors does not dependably provide an accurate indication of radiation detection performance in these material systems without further experimental information. This current situation leads to a lack of consistency in the assessment and reporting of radiation detecting metrics that makes it difficult to compare the performances of the latest materials and devices across different laboratories and applications. Such limitations impede both fundamental material advancements and the industrial translation of emerging radiation detector technologies. A similar problem was widely reported for perovskite solar cells, where the stability metrics developed for traditional photovoltaic devices were found to provide a poor method for assessing the degradation mechanism in perovskite photovoltaic systems.[31] To address this concern a group of researchers proposed a list of both additional procedures to account for properties specific to perovskites, and data to provide in publications to enhance consistency across laboratories.[32] Adoption of these guidelines for conducting stability studies have now been shown to have substantially improved comparisons between data from different laboratories and from different device architectures.

With the strong growth of research on organic and perovskite radiation detectors, there has been increasing focus on the need to standardize procedures and parameters reported. For instance, a recent report highlighted the lack of valid methodologies for determining the lower limit of detection for perovskite x-ray detectors,[33] however, similar issues are also evident across the literature for other radiation detection metrics, including sensitivity, and radiation-induced charge carrier transport, and radiation stability (**Figure 1**). In this work, we first outline some of the unique photophysical features of organic and perovskite materials, then propose a systematic and standardized approach for the determination of targeted metrics determined under conditions that are relevant to the radiation environment of specific applications. An overview of the key procedural information and protocols we suggest reporting for characterization of organic semiconductors and perovskite radiation detectors are shown in **Figure 2**. Consideration of accurate determination of these metrics, and reporting of the experimental parameters which can strongly influence them, will improve data comparison across labs and assist in identifying the key material and device properties required to advance perovskite and organic radiation detectors.

2. Fundamentals of Radiation Detection with Organic Semiconductors and Perovskites

2.1. Ionizing Radiation Interactions with Materials

The effectiveness of ionizing radiation detection is dictated by the interactions that occur between the incident radiation and absorbing material. The interaction may either cause excitation (by raising electron energy to a higher energetic state) or ionization (by removing an electron entirely from an atom). We first consider the interactions for gamma and x-ray photons, which are by far the most frequently employed sources for novel radiation detecting materials. The interaction of photons with the active layer can occur via various mechanisms, including the photoelectric effect (PE), Compton scattering (CS), or pair production (PP), depending on both the energy of the photon, E and the average atomic number of the elements in the detecting material, Z_{ave}.[37] Photon attenuation by an absorbing material is dependent on the combined probability of these interaction processes (represented by an attenuation coefficient, μ), which is characterized using a standard Beer-Lambert type relationship:

$$I = I_0 e^{-\mu x} \tag{1}$$

where I is the number of transmitted photons, I_0 the initial number of incident photons, and x is the material thickness. In the radiation detection literature, μ is often normalized by the material density, ρ to produce a mass attenuation coefficient (μ/ρ) that provides a constant value for an element for intrinsic comparison of different materials without the impact of their different material densities. When characterizing new detector materials, consideration should be given to both the magnitude of the mass attenuation coefficient, which is a key parameter in determining

 © 2025 The Author(s). Advanced Functional Materials published by Wiley-VCH GmbH

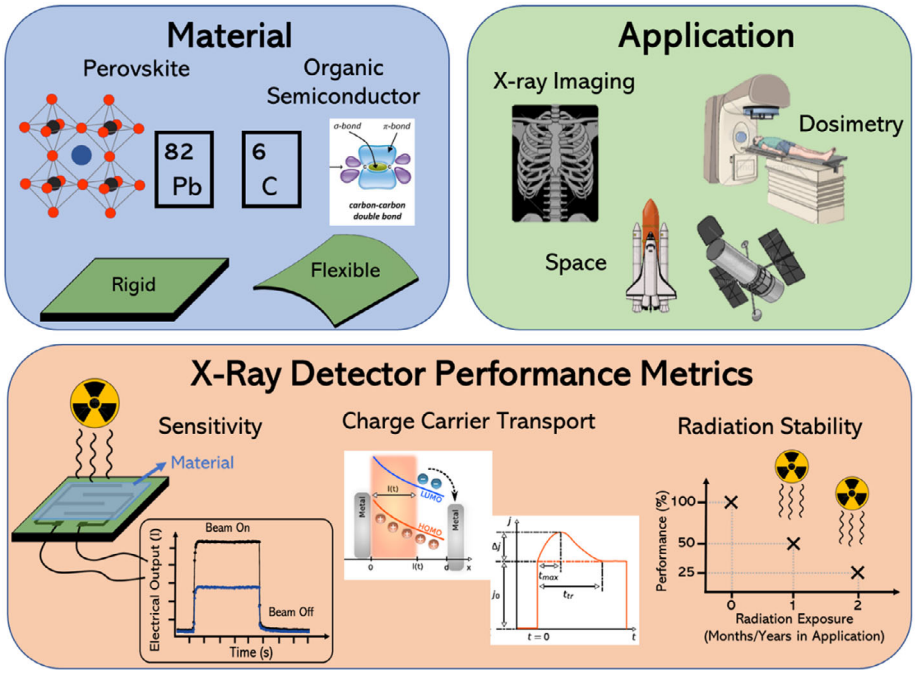


Figure 1. Illustrated summary of the active materials, range of applications and performance metrics necessary to characterize novel ionizing radiation detectors.

detector sensitivity, and the variation in this coefficient as a function of energy, which is a critical feature in determining the dynamic range of the detector. Unlike traditional radiation detector materials, organic semiconductors, and metal halide perovskites typically excel at only one of these two aspects (i.e., high attenuation or stable values across wide energies), with much greater performance trade-offs made at the expense of the other.

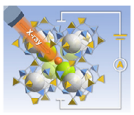
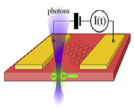
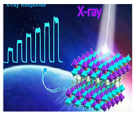
KEY METRIC	CONSIDERATIONS AND LIMITATIONS	EXEMPLAR REPORTING
SENSITIVITY 	• Linearity and energy range • Dose rate dependence • Photoconductive gain	[26], [39], [102]
CARRIER MOBILITY 	• Method of measurement • Electric field dependency • Layer thickness dependency	[26], [200], [202]
RADIATION HARDNESS 	• Number & duty cycle of exposures • Total ionising radiation dose • Radiation induced leakage current	[207], [222], [240]
IMAGING 	• Limit of detection (SNR +time) • Modulation transfer function • Detective quantum efficiency	[99], [259], [261]

Figure 2. A summary of the key metrics for characterizing organic semiconductor and perovskite radiation detectors, some experimental considerations for reporting with each metric, and examples of exemplar reporting. Images adapted with permission from references.[34–36]

2.2. Comparison of Use Cases for Organic Semiconductors and Perovskite Detectors

Figure 3a shows that the mass attenuation coefficient of lead, the most frequently employed metal in organo-halide perovskite materials, is extremely high at low energy (10–100 keV) but it is also highly non-uniform with respect to energy. The strong attenuation explains why lead-halide perovskites are attractive for new radiation detecting technologies, as it enables higher radiation sensitivities than existing inorganic detecting materials (e.g., silicon).[38] The inset of Figure 3a also demonstrates that the high-Z elements in perovskites (also including for instance iodine; Z = 53) result in the materials interacting with photon beams via the photoelectric effect across a much wider energy range than for low-Z materials.[28] Interactions dominated by the photoelectric effect also enhance the radiation sensitivity of perovskites, since the full energy of the photon is absorbed in each interaction, rather than only partial energy absorption as occurs in a CS interaction. However, this greater energy deposition may also induce greater damage in the detecting material. For example, it is well known within the medical community that while higher contrast X-ray images are achieved using lower beam energies that take advantage of enhanced PE interaction probabilities to create higher sensitivity, this PE mechanism also deposits a significantly increased radiation dose into the patient, resulting in dangerous radiobiological effects.[39]

In contrast to perovskites, organic semiconductors, which are composed predominantly of low-Z elements such as carbon, oxygen, hydrogen, and nitrogen, interact with photons predominantly via the CS mechanism, and have much lower mass attenuation coefficients.[41] However, their attenuation coefficients are also much more constant with respect to energy (Figure 3a),

 © 2025 The Author(s). Advanced Functional Materials published by Wiley-VCH GmbH

16163028, 2026, 21, Downloaded from https://advanced.onlinelibrary.wiley.com/doi/10.1002/adfm.202423521 by Adelaide University, Wiley Online Library on [30/09/2026]. See the Terms and Conditions (https://onlinelibrary.wiley.com/terms-and-conditions) on Wiley Online Library for rules of use; OA articles are governed by the applicable Creative Commons License

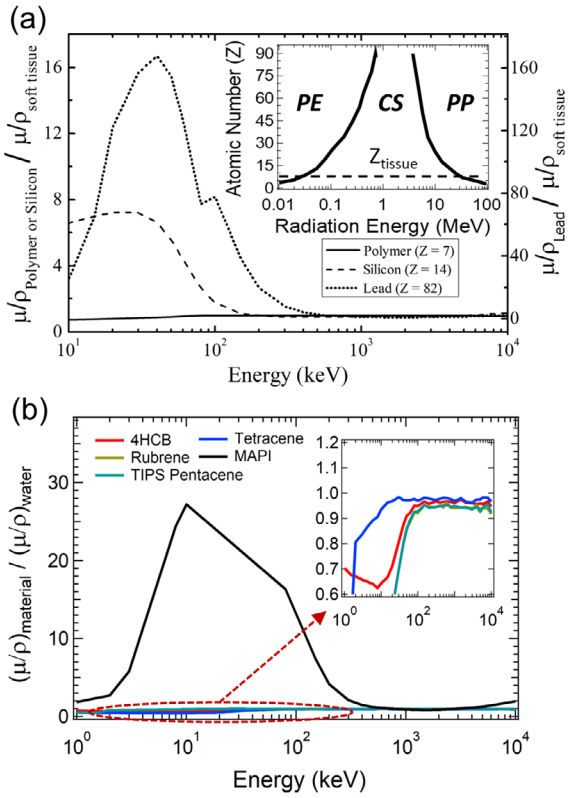


Figure 3. a) The mass attenuation coefficient (μ/ρ) of various materials to ionizing radiation of different energies compared to that of water, including organic semiconducting polymers (solid black line), crystalline silicon (dotted black line), and lead (dotted black line). The inset displays the dominant interaction mechanism between photons and the absorbing material as a function of both energy and atomic number, Z, where PE = photoelectric effect, CS = Compton scattering, and PP = pair production. Data was taken from the National Institute of Standards and Technology (NIST) database.[40] b) Values calculated for the ratio of the mass attenuation coefficient of organic semiconducting single crystals 4-hydroxycyanobenzene (4HCB), rubrene, 6,13-Bis(triisopropylsilylethynyl)pentacene (TIPS-pentacene), tetracene, and perovskite methylammonium lead iodide (MAPI) to that of water using Geant4 Monte Carlo simulations. The inset shows an expanded region for the organic single crystals around the desired ratio of 1 for water (or tissue) equivalent materials.

and fortuitously for applications in medical science and health-related dosimetry, closely mimic the absorption by human tissue (or water, which is often used as a proxy for tissue equivalency due its compositional dominance in the human body) of radiation.[42] The energy deposited by radiation in biological materials is difficult to predict when measured with substances that are not intrinsically tissue equivalent, as it requires complex calibrations that depend on energy, angle of incidence, and depth of field. Figure 3a shows the measured mass attenuation for common detecting materials with respect to water, whilst Figure 3b shows simulated values for lead halide perovskite and some common organic semiconductors that are known to form high efficiency single crystals.[43] Whilst silicon and perovskites exhibit a variation of up to 600% and 2500%, respectively, the variation of the organic semiconductors is as low as 10% across the energy range of 10 keV – 1 MeV. The low energy dependence of the radiation attenuation properties becomes an important consideration for applications in complex mixed radiation fields where a large range of energies needs to be accurately detected simultaneously.[44] Considering these properties, perovskite materials are most suited to applications where high attenuation and spatial resolution are required in a narrow energy window, with lower dose rates (<1 Gy/min) and low beam energies (10–50 keV). Current technologies matched to these properties include x-ray imaging and single particle detection. Organic semiconductors are most suited to applications with mixed radiation beams (e.g., photons, electrons and protons) and energies (e.g., multiple energies need to be recorded simultaneously), with these materials excelling in applications requiring uniform detection properties under higher dose-rates, e.g., radiation therapy, synchrotron radiation, space exploration, and nuclear energy monitoring.

Once the initial interaction process has occurred, the secondary photoelectron loses kinetic energy to generate multiple electron-hole pairs through inelastic electron–electron scattering, secondary X-ray generation, and Auger processes.[28] Due to the energy deposited through interactions with these secondary electrons, the detecting material produces an electrical signal that is proportional to the amount of energy deposited. The interactions of detecting materials with such secondary electrons are very different from the interactions described earlier for primary photon attenuation, as these electrons are charged and carry a much higher effective mass. For both ions and electrons, the linear stopping power, S, refers to the detecting materials ability to stop the charged particle by defining the kinetic energy, dE, lost as a function of distance travelled, dx, $S = -dE/dx$. Both a higher Z and a higher number density, N, of the detecting material increase the stopping power, i.e., increase the energy deposited along the path.[45] The stopping power also changes with incident radiation energy, a characteristic particularly important for the emerging area of proton detection using organic or perovskite detectors.[46,47] When assessing the electron and proton stopping power ratios for these materials, a similar trend is observed to that seen in Figure 3. **Figure 4** shows simulated results for perovskites and organic semiconductors modelled using Monte Carlo methodologies, where the perovskite response is found to vary greatly with energy with respect to the response of water, from 50–200% for electrons and 100–400% for protons in the energy window of 1 keV to 1 GeV. In contrast, organic semiconductor materials interact with protons in a similar manner to water across the same energy range.

The implication of this fundamental radiation-induced photophysics for perovskites and organic semiconductors is that the reporting protocols for conveying the response and associated characterization of detector materials must be measured and reported in detail sufficient to reproduce the beam properties of the intended application. For example, energy-dependent materials like perovskites are well-suited for detecting a monochromatic or narrow bandwidth x-ray source, though given their strong energy dependence, the energy spectrum of the source should be fully characterized and reported. This reporting should also be accompanied by details of the accelerating voltage and beam current used to produce the radiation source (or if using radioactive emissions, the activity of the source at the time of measurement) to allow comparisons between laboratories at the same

© 2025 The Author(s). Advanced Functional Materials published by Wiley-VCH GmbH

16163028, 2026, 21, Downloaded from https://advanced.onlinelibrary.wiley.com/doi/10.1002/adfm.202423521 by Adelaide University, Wiley Online Library on [30/09/2026]. See the Terms and Conditions (https://onlinelibrary.wiley.com/terms-and-conditions) on Wiley Online Library for rules of use; OA articles are governed by the applicable Creative Commons License

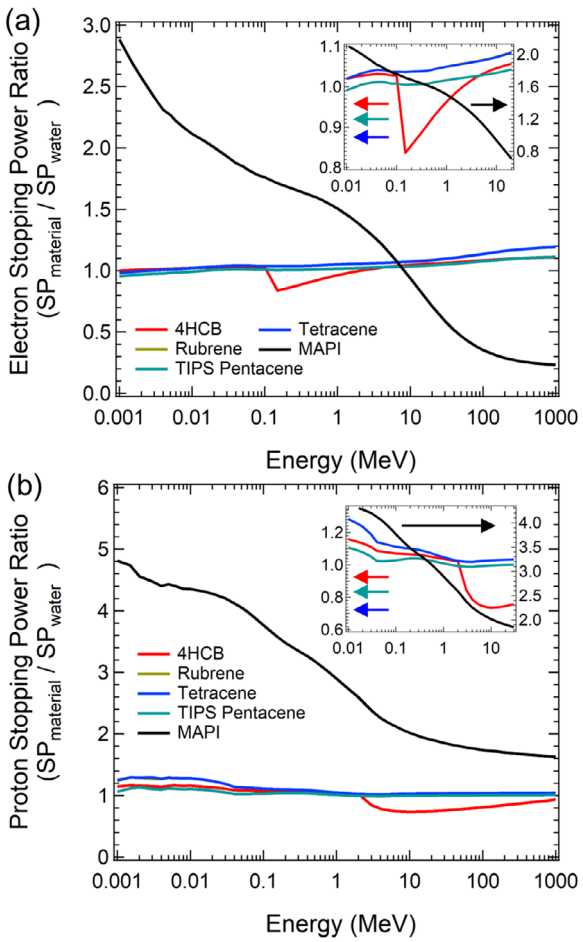


Figure 4. Values calculated for the ratio of the a) electron stopping power, and b) proton stopping power of organic semiconducting single crystals 4-hydroxycyanobenzene (4HCB), rubrene, 6,13-Bis(triisopropylsilylethynyl)pentacene (TIPS-pentacene), tetracene, and perovskite (MAPI) to that of water using Geant4 Monte Carlo simulations.[48] The inset shows an expanded view of the energy regime most frequently utilized by these next-gen detector materials.

energies and beam flux. In applications for dosimetry, the energy dependence, which is often overlooked in the literature, becomes a critical parameter, and should be fully characterized and reported across an energy range from 10 kV to 6–15 MV.

2.3. Radiation Induced Charge Generation and Transport Models

Crystalline detector materials traditionally employed for radiation detection are described by well-defined electronic band structures. Charge transport is well explained by the Shockley-Read-Hall generation and recombination model, where the electron transitions between band states of the semiconductor using differing energy levels created by dopants or defects (referred to as traps).[49,50] The radiation-induced charge generation and transport processes in crystalline detector materials are thus well understood, and with an appreciation of enhanced surface defects and the need for their passivation,[51] these principles can be reasonably applied to perovskite materials to understand and interpret the detector responses.[52–54] In contrast, charge separation, recombination, and transport in organic semiconducting materials are typically explained by theories that specifically consider the localized nature of charges (e.g Onsager-Braun theory, polaron theories, and random-walk time models).[55–57] Whilst these models are often used to explain behavior in the literature, they were developed for low intensity optical excitations. It is not clear whether the typical assumptions of these models, when applied to visible-light excitation, are directly applicable to high-energy radiation and at high dose rates. For example, under high energy radiation, multiple charge generation leading to highly charged segments of a semiconductor could be expected.[58,59] Although investigated several decades ago for early conducting polymers, to date, there have been limited studies exploring charge generation and recombination mechanisms in modern organic semiconducting materials under high energy irradiation,[60] and those studies that have been performed have detected significant anomalous behavior, such as intrinsic gain creation[61] or compression.[62] From these studies, it appears that existing theories of charge generation, transport, and recombination in non-crystalline emerging detector materials, developed primarily for explaining the photophysics under low energy optical irradiation, will need to be revised or new theories will need to be developed in order to accurately predict their response under ionizing radiation.

2.4. Radiation Detection Mechanisms

Ionizing radiation can be detected through two different mechanisms, referred to as direct or indirect detection (**Figure 5**). Direct detection uses a material, commonly a semiconductor, to first absorb the incident radiation and convert it into electrical charge, then second to transport the charge out of the semiconductor to produce an electrical signal.[63] High-Z crystalline materials like perovskites are suited for direct detection as they maximize both charge creation (due to high attenuation coefficients) and charge transport (due to high mobilities) in the same material.[64] Direct detection has been the subject of intense recent interest with perovskites, resulting in several studies focusing on achieving the detection sensitivities that are higher than currently available technologies.[65–69] However, comparisons between these studies should account for the energy dependence and flux variations that could strongly influence reported sensitivity values as outlined in Section 2.2 and discussed in further detail in Section 3. Furthermore, several of these studies are performed using differing device architectures. Since the charge transport and general device response to radiation is known to be influenced by the detector architecture for perovskites and organic semiconductors, one of the key considerations to enable direct comparison of different results is to determine whether the reported results are driven predominantly by the material response, the device architecture, or a combination of the two factors, which requires testing with multiple materials and/or device architectures to obtain a valid control measurement.[70]

Indirect detection uses a scintillating material to first convert ionizing radiation into optical photons. A secondary photosensitive layer can then transform the optical photons into an electrical output. An advantage of the indirect detection mechanism

© 2025 The Author(s). Advanced Functional Materials published by Wiley-VCH GmbH

16163028, 2026, 21, Downloaded from https://advanced.onlinelibrary.wiley.com/doi/10.1002/adfm.202423521 by Adelaide University, Wiley Online Library on [30/09/2026]. See the Terms and Conditions (https://onlinelibrary.wiley.com/terms-and-conditions) on Wiley Online Library for rules of use; OA articles are governed by the applicable Creative Commons License

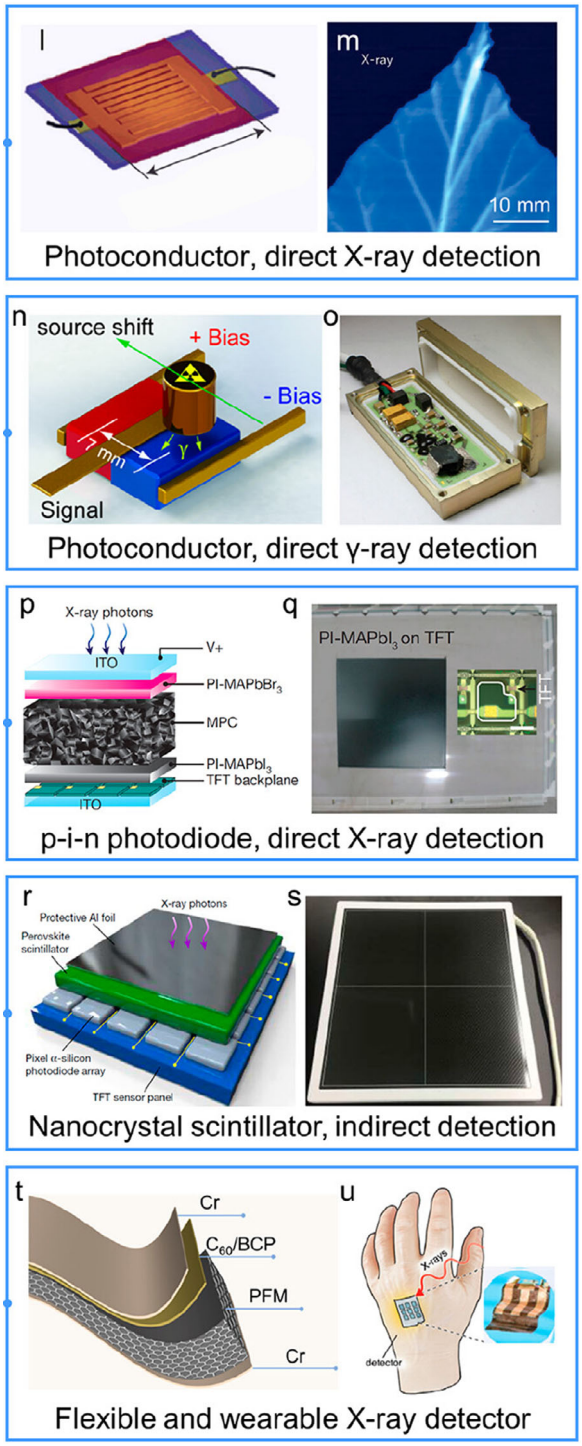


Figure 5. The various device architectures of organic semiconductor and perovskite radiation detectors are utilized in direct and indirect detection modes. Images adapted with permission from references.[12,38,71–74]

is that the radiation absorption and the charge carrier extraction functionalities of the detector can be independently optimized in the scintillator and photosensitive layers, respectively.[23] Decoupling detection requirements of strong attenuation and high radiation hardness from the electrical features of efficient charge transport and extraction, and collection enables a test-bed with a wide plethora of appropriate materials.[75–82] However, it is worth considering that indirect detection can reduce some performance metrics, e.g., the spatial resolution of a pixelated device due to its isotropic emission that induces crosstalk between neighboring pixels. Whilst advanced research concepts such as photonic crystals for directing the scintillator emissions have been proposed to address this limitation, such shortcomings will be important for applications in small field dosimetry or imaging applications. Therefore, as for the detecting materials themselves, the intended application of the radiation detector dictates the detection mechanism, either direct or indirect, in addition to the detecting material.

3. Sensitivity as a Key Metric for Organic Semiconductor and Perovskite Radiation Detectors

The design and evaluation of radiation detectors involves numerous parameters, each contributing to the overall performance of the device. Whilst the selection of the active material based upon key intrinsic properties such as mobility, carrier lifetime, bulk resistivity, and atomic number is often a primary focus for radiation detectors, complexities arise in a detector structure due to the electronic states at the interface between electrodes and additional layers commonly employed in both perovskite and organic X-ray detectors.[83,84] Interlayers are used to selectively transport electrons and holes to their respective collecting electrodes, and when optimized, have been a fourfold increase in the detector's sensitivity due to improved transport at the grain boundaries with the active layer.[85] Furthermore, organic semiconductors and perovskites exhibit significantly higher levels of structural disorder, bulk trap densities, and surface states than inorganic materials, which can often vary with fabrication procedures where their influence may not be fully captured by intrinsic material-level metrics.[86–89] Accordingly, macroscale device parameters that reflect the device performance are strongly recommended as the primary key metric to determine a detector's suitability for a given application.

3.1. Sensitivity

Sensitivity (S) refers to the ability of the detector to respond to the presence of an external radiation signal by analyzing the amount of electrical charge collected (Q) per unit radiation exposure (the absorbed dose, D). Higher sensitivity allows for the detection of weaker signals and lower levels of radiation, particularly desirable in medical applications as it allows a lower dose to be delivered to the patient.[90]

$$S = \frac{Q}{DA} \tag{2}$$

The sensitivity is generally expressed as a function of the detector geometry, though in the literature this normalization is frequently varied between a unit area and a unit volume. Thus, care should be taken when comparing sensitivity values reported in the literature for different materials and devices. The use of sensitivity per unit volume highlights the intrinsic material properties,

© 2025 The Author(s). Advanced Functional Materials published by Wiley-VCH GmbH

16163028, 2026, 21, Downloaded from https://advanced.onlinelibrary.wiley.com/doi/10.1002/adfm.202423521 by Adelaide University, Wiley Online Library on [30/09/2026]. See the Terms and Conditions (https://onlinelibrary.wiley.com/terms-and-conditions) on Wiley Online Library for rules of use; OA articles are governed by the applicable Creative Commons License

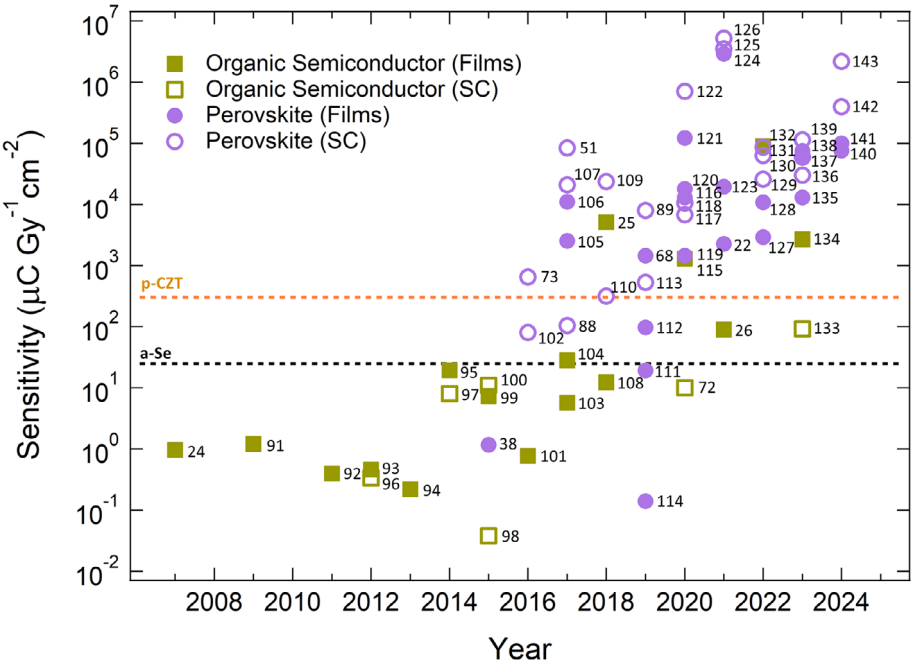


Figure 6. A recent timeline of improvements in reported sensitivity values for organic semiconducting and perovskite radiation detectors operated in direct detection modes. The values for current commercial inorganic technologies of amorphous selenium and polycrystalline CZT are shown for reference. Data values have been extracted from references [22,24–26,38,51,62,68,72,73,88,89,91–143] with the corresponding references indicated to the right of each data point.

and thus often produces high values for organic semiconductors and perovskites, where the film thickness of operational devices is on the scale of $10^{-6} - 10^{-7}$ m, in comparison to inorganic materials, where the film thickness for detectors is typically orders of magnitude larger ($\approx 10^{-3} - 10^{-4}$m). In comparison, the use of sensitivity per unit area highlights the complete performance of an operational device. Since sensitivity is used to convey a metric for macroscale detector performance, a normalization per unit area is the suggested figure of merit for this metric. The normalizing area should be determined for the entire device and not simply the active channel area (i.e., the product between the channel width and the channel length) for interdigitated electrodes to be fairer in the comparison between devices with different geometries, such as planar devices or stacked multilayer detectors.

Experimentally, it is often simpler to measure the instantaneous current in response to radiation rather than the total photoinduced charge as a function of cumulative dose. In this case, the unit of radiation exposure becomes the dose rate $(\dot{D})$ to account for the corresponding time dependence of the charge inherent in the measured current in the numerator:

$$S = \frac{I_{radiation} - I_{dark}}{\dot{D}A} \tag{3}$$

The sensitivity values reported for organic semiconductors and perovskite radiation sensors in recent years are shown in **Figure 6**. This data appears to demonstrate a trend of rapidly improving sensitivity values for both materials, though it is painstaking to extract and standardize due to the inconsistent measurement and reporting protocols for sensitivity. Thus, a renewed consideration of accurate reporting of this metric to allow valid comparisons into the future is of high importance to the field.

Sensitivity can be thought of as analogous to an external quantum efficiency that is often used to characterize photodiode detectors.[144,145] S is a product of the attenuation quantum efficiency, η_x (number of photons absorbed by the material), the charge carrier generation efficiency (number of electron-hole pairs produced per absorbed photon), η_g, and the charge collection efficiency (number of electron-hole pairs extracted per generated pair), η_{cc} multiplied by a pre-factor S_0 that is dependent on the photon energy. The attenuation efficiency can be derived in a straightforward manner from Equation (1) as:

$$\eta_x = 1 - e^{-\mu L} \tag{4}$$

where μ is the linear attenuation coefficient and L is the device thickness. For ionizing radiation, the number of charge carriers (electron-hole pairs) produced per absorbed photon is related to the incident energy entering the material, E, the energy required to create an electron-hole pair in a material, $W_{\pm}$, and the energy absorption coefficient, μ_{en}, which is the proportion of the initial photon energy that is locally transferred to the material through ionization and excitation:

$$\eta_g = \frac{E\left(\frac{\mu_{en}}{\mu}\right)}{W_{\pm}} \tag{5}$$

The charge collection yield can typically be determined from comparing the carrier diffusion length to the device thickness, as will be discussed further in the following section. Several more comprehensive discussions of maximum theoretical sensitivity

© 2025 The Author(s). Advanced Functional Materials published by Wiley-VCH GmbH

16163028, 2026, 21, Downloaded from https://advanced.onlinelibrary.wiley.com/doi/10.1002/adfm.202423521 by Adelaide University, Wiley Online Library on [30/09/2026]. See the Terms and Conditions (https://onlinelibrary.wiley.com/terms-and-conditions) on Wiley Online Library for rules of use; OA articles are governed by the applicable Creative Commons License

can be found elsewhere,[146–149] though it is recommended that this value be estimated and compared to the measured sensitivity to help determine the validity of the experimental values. In a practical sense, Equation (5) alone can serve as an upper estimate for the maximum sensitivity, since the values of η_x and η_{cc} cannot exceed unity. There are some photophysical mechanisms that may cause the experimental sensitivity to exceed the maximum theoretical value, though there are also multiple experimental factors that can artificially skew a reported experimental sensitivity to unrepresentative quantities if not carefully considered.

3.1.1. Energy Dependence

Section 2.1 described how the attenuation coefficient and cross section of a material are dependent on both the atomic number and the incident radiation energy. Accordingly, the sensitivity will also show a strong dependence on the photon energy at which it is measured, typically returning lower values for higher energies as highlighted in Figure 3. Therefore, there is a detector design trade-off between using high-Z materials to tune for high sensitivity in a specific energy window versus using low-Z materials to achieve a relatively uniform sensitivity across different energies. The traditional focus in the literature has been on designing detectors for ultra-high sensitivity, however, when comparing measured sensitivities to other previously reported values, such as the data presented in Figure 6, this energy dependence should be considered, particularly where the measurement energy may not align directly with the stated application of the detector. For instance, a very high sensitivity at lower energies may not be an advantageous metric in certain imaging applications if the sensitivity varies strongly across a relatively narrow energy range, since to reconstruct the X-ray field in an image, there are typically different energies required. Such an issue may be able to be remedied using software corrections by applying an energy-dependent calibration to correct for sensitivity variation,[150,151] however, this becomes impractical for applications with mixed radiation fields and wide energy ranges, e.g., space and radiotherapy. The native energy dependence could also be varied using materials that introduce photoconductive gain to the sensitivity rather than relying on the intrinsic responsivity, however, this will also produce a higher dark current and signal-to-noise ratio, and thus it would not facilitate use with the lower dose rates required for medical imaging.[152]

3.1.2. Linearity

As highlighted in Equation (2), the sensitivity of a detector is dependent on the charge output per unit of radiation dose (or in the differential form of Equation (3), current output per unit dose rate). For an ideal detector, this ratio remains constant across a wide dose/dose rate range, however, it has been well-established that traditional radiation detectors often exhibit non-linear responses with respect to radiation dose, particularly at the extremes of low or high dose rates.[153,154] This dose rate dependence has not yet been investigated in detail for emerging materials such as organic semiconductors and hybrid perovskites, though the effect is known to vary markedly (and unpredictably) in silicon materials as a function of the doping and radiation damage.[155,156] It is likely that devices fabricated using disordered materials like organic semiconductors and perovskites would experience substantial non-linearity in the sensitivity as a function of both instantaneous dose rate in a single measurement and cumulative dose rate across multiple characterization procedures.[157] Accordingly, we suggest best practice for determining sensitivity is to measure the charge output (or current) of a device as a function of a wide range of cumulative doses (or dose rates) relevant to the application of the detector. Ideally this plot would exhibit a linear relationship from which the sensitivity can be extracted from the slope, though for non-ideal devices it would highlight regions of non-linearity where the reported sensitivity is far less reliable as a detector performance metric.

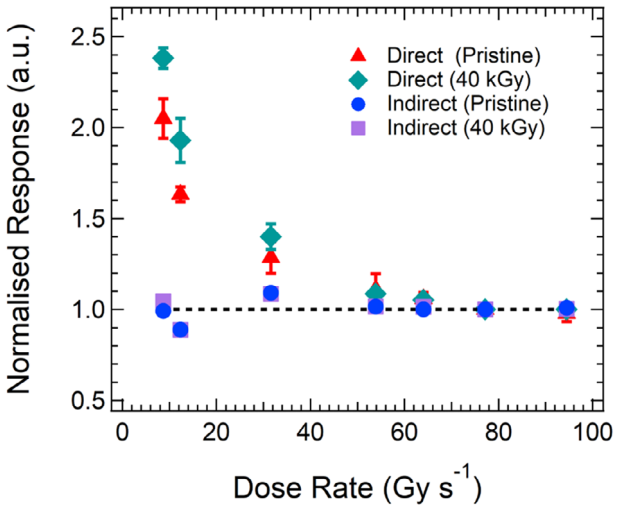


Figure 7. The influence of cumulative dose (pristine detectors and re-measurement following 40 kGy of radiation exposure) and detector architecture (direct detection and indirect detection via coupling with a 2 mm BC400 scintillator) on the dose rate dependence of an X-ray detector made with an organic semiconductor active layer (P3HT:PCBM).

We also note that dose rate dependent sensitivity is hypothesized to be a function of radiation-induced non-linear carrier dynamics in photoconductive materials. Therefore, one potential method to avoid such non-linear sensitivities is to move to an indirect detection mode where the high-energy photons are down-converted to optical energies prior to electrical detection.

This strategy has been successfully shown to convert non-linear direct device responses into linear responses for organic semiconductors, regardless of high levels of cumulative pre-irradiation to change the doping levels (**Figure 7**). There are also reports in the literature that the use of scintillators coupled to photodiodes for indirect detection produces highly linear responses for other next-gen devices, including perovskites,[158] metal organic frameworks,[159] and optical fiber detectors.[160] However, disordered semiconductors are also known to exhibit non-linear responses to high intensities of visible light illumination, a phenomenon referred to as dynamic-range enhancing gain compression.[161] Thus, whilst the influence of dose rate dependence can be mitigated by down-conversion to optical photons using indirect sensitization, if the incident flux is extremely high, non-linear responses to visible light could still persist.

© 2025 The Author(s). Advanced Functional Materials published by Wiley-VCH GmbH

16163028, 2026, 21, Downloaded from https://advanced.onlinelibrary.wiley.com/doi/10.1002/adfm.202423521 by Adelaide University, Wiley Online Library on [30/09/2026]. See the Terms and Conditions (https://onlinelibrary.wiley.com/terms-and-conditions) on Wiley Online Library for rules of use; OA articles are governed by the applicable Creative Commons License

16163028, 2026, 21, Downloaded from https://advanced.onlinelibrary.wiley.com/doi/10.1002/adfm.202423521 by Adelaide University, Wiley Online Library on [30/09/2026]. See the Terms and Conditions (https://onlinelibrary.wiley.com/terms-and-conditions) on Wiley Online Library for rules of use; OA articles are governed by the applicable Creative Commons License

3.1.3. Photoconductive Gain

The sensitivity can be thought of as analogous to a classic responsivity metric for photoconductive detectors, where a semiconductor is placed between two ohmic contacts. Accordingly, it would be expected that the sensitivity will be proportional to the mean lifetime of carriers generated under high energy radiation, that is, longer lived carriers can contribute to the detector photocurrent for longer times, and inversely proportional to the transit time of carriers, that is, the faster carriers move through the device, the more they contribute to the current output.[162] This combination of carrier transit time and lifetime is often captured by a metric known as photoconductive gain, G_p:

$$G_p = \frac{\tau_r \mu V}{d^2} \tag{6}$$

where τ_r is the carrier lifetime, μ the charge carrier mobility, V the voltage applied to the detector, and d the distance between the detector electrodes. Importantly, the photoconductive gain can reach values substantially larger than unity, which means that the obtained photocurrent for a given radiation dose rate (i.e., the sensitivity) can be amplified by factors that are both intrinsic to the detecting materials (τ_r, μ) or extrinsic factors dependent on the device architecture and characterization procedure (V, d). It is therefore foreseeable that detectors made from an identical semiconductor could return greatly different sensitivity values depending on device architecture or applied bias in the measurement. Equally, since the carrier lifetime and mobility are functions of material properties such as defects and traps, surface states and depletion regions that can localize minority carriers,[163] and these effects are known to be particularly prevalent in organic semiconductors and perovskites,[164,165] it is also possible that detectors made with nominally identical active layers and architectures could return different sensitivities depending on the specific fabrication protocols used to deposit the materials in different laboratories. Indeed, high sensitivity values in organic semiconductor[101] and perovskite[38] radiation detectors found in recent reports can only be accounted for by considering substantial photoconductive gain as a dominant detection mechanism. Such intricacies can make direct comparison of sensitivity values across different studies in the literature complex, particularly for emerging materials with high levels of intrinsic disorder. We therefore suggest that either the gain itself, or the fundamental parameters that are used to determine it, should also be reported alongside sensitivity characterizations to facilitate the nuances involved in comparing devices to be transparently considered (noting that measurement of some of these metrics is itself complex and will be considered further in the next section).

It is also worth noting that other extrinsic device factors can influence the photoconductive gain. When fabricating detectors using a phototransistor structure in place of a photoconductor, the sensitivity can be significantly amplified due to an enhancement of the gain by polarizing the gate electrode.[103,108] Such endeavors can amplify the sensitivity to offset other desirable operational features that would typically reduce sensitivity (e.g., operation at reduced bias voltages, fabrication on flexible plastic substrates). However, caution should be taken when comparing sensitivity values across device architectures as the amplification in photoconductive gain can be substantial in phototransistors and may cause misleading comparisons of material suitability for radiation detection if not properly considered.

3.2. Update on Sensitivity of Perovskite Radiation Detectors

Most of the perovskite-based direct radiation detectors presented in the literature have to date been fabricated with a diode-like structure. The preference for this device architecture is primarily due to the previous knowledge developed under the framework of perovskite-based photovoltaics research over the past decade. Operating the photodiode in reverse bias conditions results in a low limit of detection thanks to the suppressed dark current and consequent high signal-to-noise ratio, typical of diode architectures.[116] However, in a recent study, Jia et al. demonstrated that even under reverse bias, p–i–n structured halide perovskite-based X-ray detectors showed abnormal responses to radiation and a high photoconductive gain factor.[166] The authors attributed this behavior to ion migration and accumulation in the perovskite material, inducing sharp band bending and charge tunneling at the interfaces with electrodes, which will then reduce the contact resistances, causing the device to work as a photo-conductor rather than a photodiode under reverse bias conditions. Some studies have exploited the potential of the diode structure to collect charges utilizing an internal built-in field of the junction, which enables fully-passive operation without any applied external bias,[74] an appealing feature to target low power consumption and to minimize instability issues related to ion migration that are typically triggered by bias application.[167]

In recent years, there has been extensive interest directed toward 2D perovskites due to their superior environmental and thermal stability, reduced ion migration, and low defect density.[168,169] These materials have been developed as radiation detectors not only as photodiodes,[116] but also in photoconductor architectures.[170] The absence of rectification in photoconductor architectures is in fact, compensated by the higher bulk resistivity, i.e., lower dark current of 2D perovskites with respect to their 3D counterparts.[171] This approach has been proposed both for planar[172] and vertical geometries,[173] with excellent detection performance in terms of sensitivity, stability, and detection limits.

On the other hand, besides the stability improvement, 2D perovskites limit two of the strongest advantages of employing perovskites instead of organic semiconductors as active layers for the detection high-energy photons, i.e., improved carrier transport properties and higher radiation stopping power thanks to their higher density. Combining perovskites with different dimensionalities has been proposed as a strategy to overcome such limitations. Xu et al. reported on direct X-ray photoconductive detectors based on 2D/3D double layer perovskite films, where a 2D material with phenylethylammounium (PEA) and methylammounium (MA) cations and lead iodide base [$(PEA)_2MA_3Pb_4I_{13}$] layer is deposited parallel to the substrate is cascaded with a vertically grown 3D $MAPbI_3$ layer.[123] In this double structure, the 2D perovskite stabilizes the current baseline, suppressing the ion migration, and the presence of 3D perovskite ensures fast carrier transport, leading to high values of sensitivity.

© 2025 The Author(s). Advanced Functional Materials published by Wiley-VCH GmbH

16163028, 2026, 21, Downloaded from https://advanced.onlinelibrary.wiley.com/doi/10.1002/adfm.202423521 by Adelaide University, Wiley Online Library on [30/09/2026]. See the Terms and Conditions (https://onlinelibrary.wiley.com/terms-and-conditions) on Wiley Online Library for rules of use; OA articles are governed by the applicable Creative Commons License

3.3. Update on Sensitivity of Organic Semiconductor Detectors

The approach to conceiving the architecture for a direct X-ray detector based on organic semiconductors is forced to be different from perovskites due to the lower radiation attenuation in these materials. Despite several studies reporting on photodiode architectures for organic X-ray detectors reaching appropriate low dark currents and low limit of detection,[104,174,175] these structures have not produced the same high sensitivity values produced by perovskite devices. The introduction of heavy elements blended into the organic matrix to increase the absorption of high energy photons has been trialed,[94,176–178] however, such composites resulted in a loss of the intrinsic human tissue equivalence of organic compounds, a unique feature that makes this class of materials very appealing for dosimetry applications. The development of organic direct X-ray detectors in photoconductor or phototransistor geometry has therefore become preferred for maximizing sensitivity values. In this case, the detection process is dominated by high photoconductive gain, which leads to very high sensitivity values and allows for easily measurable signal amplitudes despite the high dark current typical of photoconductor architectures.[101,103] Following this approach, it is possible to conceive and realize a highly sensitive radiation detector with a fully organic tissue equivalent active layer. When the detection process is dominated by a photoconductive gain effect, a phototransistor architecture allows full control of the detector performance. The presence of a third electrode controlling the field effect in fact tunes the charge density in the transistor channel, bringing enhancement of charge accumulation and gain of the detection signal. This phenomenon, combined with different possible strategies to boost charge carrier mobility of organic semiconductors (by chemical synthesis,[108] or by deposition processing and trap passivation[115]), led to outstanding sensitivity values being reported in organic thin film transistor-based X-ray detectors, largely surpassing those reported for two-terminal architecture devices based on both organic and perovskite thin films.[132] Whilst these approaches have led to increasing sensitivity values for organic semiconductors, these materials still underperform in imaging and charge spectroscopy applications compared to perovskites, although they are much better suited to calibrated dosimetry. A novel approach to bring the best of these two materials systems together has been proposed by Gao et al., who reported on a hybrid organic/perovskite heterojunction X-ray phototransistor.[66] Such devices exploit the high X-ray mass attenuation coefficients of Caesium lead bromide ($CsPbBrI_2$) nanocrystals and the highly efficient charge transfer at the perovskite/organic heterointerface to obtain an X-ray detector combining high sensitivity with low detection limit.

4. Charge Carrier Transport as a Key Metrics for Organic Semiconductor and Perovskite Radiation Detectors

Charge carrier transport is a key property utilized to characterize radiation detectors. The physical parameters most often used for this purpose are the mobility or the lifetime of charges in a device. These metrics are powerful because they are simple. However, determining them in operating devices and research-grade materials is fraught with complexity and can result in misleading comparisons between different materials and device architectures. Accordingly, the use of charge transport measurements as radiation detector performance metrics needs to be considered and interpreted, particularly to clarify whether the measured values provide information about material optimization, device architecture optimization, or a combination of both activities. In the remainder of this section, some commonly used experimental techniques to measure carrier transport are discussed in the context of their specific measurement requirements to produce accurate and reliable data for radiation detectors.

4.1. Mobility – Lifetime Product

A fundamentally important metric of a photodetector material is the mean distance photogenerated carriers travel in the material before they recombine. This distance, which can be expressed as both a drift or a diffusion length, λ, varies by orders of magnitude between various semiconductors, e.g.,>100 µm in high purity silicon to < 200 nm in disordered organic semiconductors.[179] The drift length can be calculated from Equation (7)

$$\lambda = \mu\tau \times E \tag{7}$$

The drift length is driven by the product of the carrier mobility (μ) and lifetime (τ) and the applied electric field, E. From Equation (7) it can be deduced that charge transport of materials used in photodetectors can be either mobility- or lifetime-limited. In each case, the transport is potentially restricted, such that the carrier drift lengths are less than the full depleted sensor thickness, and the induced signals are reduced. Traditional radiation detector materials such as CdTe are generally lifetime limited,[180,181] whereas perovskites show very long lifetimes and are typically mobility limited.[182,183] In disorder-dominated materials such as organic semiconductors, the link between lifetime and mobility is an open research question, however, the recombination rate is often assumed to be limited by charge mobility (Langevin recombination), i.e., the probability for the charges to meet in space is the bottleneck, and not the actual electron – hole annihilation step.[184] Accordingly, the use of mobility alone can be an unreliable metric for comparing different detector performance since enhancing charge mobility may not actually increase the carrier drift length in materials and devices where the transport-controlled lifetime proportionally shortens.[185]

In the presence of screening of the external electric field, the transport in these materials may become diffusion dominated. The diffusion length is calculated from Equation (8):

$$l_d = \frac{k_B T}{e}\mu\tau \tag{8}$$

where k_B is the Boltzmann constant, T is the absolute temperature, and e is the electric charge. Whether drift or diffusion-dominated, the use of mobility and lifetime values to characterize transport is powerful; however, determining them accurately in new materials and operational devices can be challenging. First, in materials such as organic semiconductors and perovskites that exhibit either energetic disorder (distribution in the energy of the

© 2025 The Author(s). Advanced Functional Materials published by Wiley-VCH GmbH

charge transport sites, i.e., traps or segments of conjugated organic molecules)[186] or spatial disorder (variation in the site orientation/wavefunction overlap influencing electronic coupling between the charge transporting sites),[187] mobility values that depend on charge density and the magnitude of the applied electric field are often observed, both manifested in an apparent film thickness dependence of the measured mobility. Because photodiodes, photoresistors, and phototransistors can operate in vastly different electric field, charge concentration, and optimal thickness regimes, the reported mobility values are often dependent not only on intrinsic material properties, but also strongly influenced by device architecture. Thus, reporting single-point mobility values often has limited scientific use for comparing materials systems outside the specific operating range and the type of devices the measurements were performed on. Consequently, simultaneous reporting of the charge carrier concentration and electric field dependence of mobility is highly desired for accurate comparisons. Furthermore, checking the active layer thickness dependence of the measured mobility is a recommended practice, as an apparent thickness dependence is a good indicator that some experimental requirements are not strictly met.

4.2. Considerations for Mobility Measured by Space Charge Limited Current (SCLC)

Charge mobility can be derived from the current – voltage behavior of diodes and transistors under specific operational regimes (see further details in Supporting Information). The derivation of mobility values from these characterizations is convenient as they can be performed on the same device used for sensitivity measurements with the same instrumentation, however, they are also prone to errors due to non—idealities such as disorder, non-ohmic behavior of contacts, and diffusion contributions to the current, which are all factors likely to be present in perovskite and organic semiconducting radiation detectors.[188] The combined effect of several different influences on device photophysics may still manifest in the slope of the log$J$ versus log$V$ graph exhibiting a value of 2 at some region in the curve, but the resulting mobilities can be severely misinterpreted since the physical origin of these effects are not from space charge limitations, but remain unidentified due to the incorrect assumption of space charge origins.[188] Checking the thickness dependence of the mobility can be particularly useful in this instance due to the more easily distinguishable dependency of the space charge limited current on sample thickness ($J \sim d^{-3}$). However, the thickness dependence can also be complicated by morphology changes between thicker and thinner films, a particular issue for solution-processed materials like perovskites and organic semiconductors. For example, spin coating using more concentrated solutions or slower spin speeds to achieve increased film thicknesses for improved radiation detection can lead to slower evaporation, and consequently more time for material domains to crystallize. Charge mobilities can also be derived both from the linear or saturation regime of field effect transistors,[189] though a detailed description of the equations and measurement procedures is not included here. However, we do note that FET mobilities measured for disordered semiconductors can be orders of magnitude higher than those determined for the same materials in photodiode structures due to the much higher gate-induced charge densities in the transistor channel in comparison to typical diode structures.[190] Researchers aiming to compare FET mobility values to values derived from the time-resolved measurements discussed in this perspective are directed to other critical discussions and reviews available in the literature.[189]

4.3. Considerations for Mobility Measured by Time of Flight (TOF)

Time of flight (TOF) is a well-established technique for the dynamic measurement of drift mobility of charge carriers. It is particularly suitable for high resistivity bulk materials such as organic or perovskite materials, able to extract individual mobility values for electrons and holes by careful choice of the device geometry and irradiation configuration. The TOF method requires the creation of a small number of free carriers by some form of irradiation, typically achieved with an above-bandgap laser pulse, an electron beam pulse, or alpha particles. The TOF mobility is measured from the carrier drift velocity v_{dr}, as described in the Supporting Information. When the carriers reach the device contact the current pulse terminates, typically providing a distinctive peak indicative of the transit time (**Figure 8**).

The TOF method relies on three main assumptions:

1) The measured carrier transit time (τ_{tr}) is not trap-limited, (all photogenerated carriers reach the electrodes, and so have travelled a known thickness of material).
2) The electric field strength is uniform throughout the device.
3) The charge injection rate is sufficiently low that the device is not operating in a space charge limited mode.

A simple analysis of TOF pulse shapes assumes that the field is uniform through the depth of the sample, and so the drift velocity of the carriers through the device is constant. In many organic or perovskite materials, the field depth profile may not be constant, for example, due to band bending or barrier heights at the metal contacts. Additionally, the field profile may not be stable with time, for example, due to the build-up of space charge under one contact in a perovskite device due to movement of ions over time (so-called "polarization" effects). Analysis of the TOF pulse shapes can give information about the non-uniformity of the field depth profile. **Figure 9** shows an example of TOF pulses in lead halide perovskite crystals, where the amplitude of the TOF pulse increases with time, due to increasing electric field under one contact of the device. Similarly, the decay of a TOF current pulse when the charge drifts across the device is incompletely can also give an estimate of the effective carrier lifetime.

In general, the application of the TOF method is more complex for materials where either the carrier lifetimes are short or the carrier mobility is low. In the case of materials with short carrier lifetimes such as organic semiconductors, the measured transit time of the charge carriers is limited by the effective carrier lifetime. In this case, the carriers do not fully drift to the device contacts, and the drift length is less than the device thickness (ie. $l_D < d$). In this regime the experimentally observed value of τ_{tr} does

© 2025 The Author(s). Advanced Functional Materials published by Wiley-VCH GmbH

16163028, 2026, 21, Downloaded from https://advanced.onlinelibrary.wiley.com/doi/10.1002/adfm.202423521 by Adelaide University, Wiley Online Library on [30/09/2026]. See the Terms and Conditions (https://onlinelibrary.wiley.com/terms-and-conditions) on Wiley Online Library for rules of use; OA articles are governed by the applicable Creative Commons License

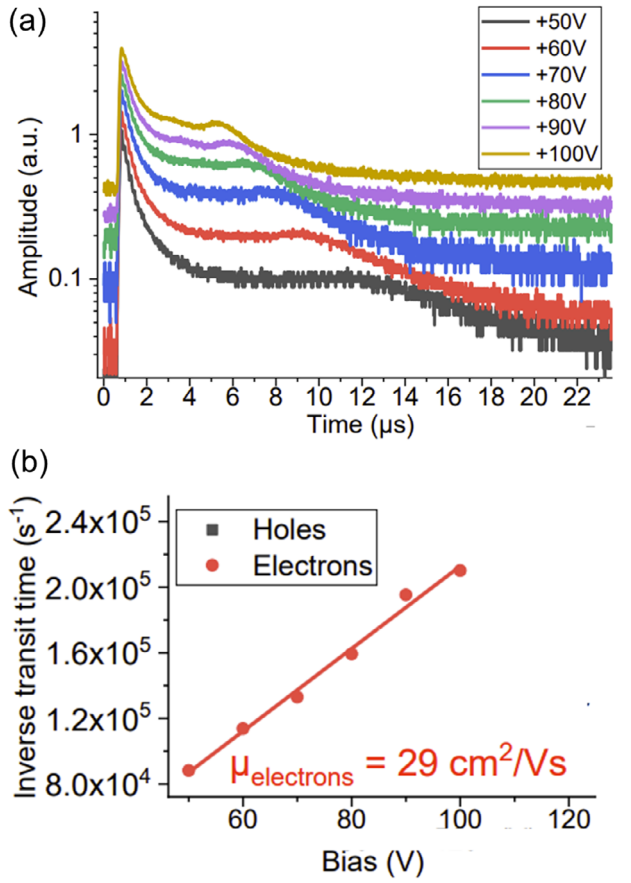


Figure 8. a) The current transients detected from a lead halide perovskite single crystal device using laser pulses. b) Extraction of the electron mobility from the TOF current pulses.

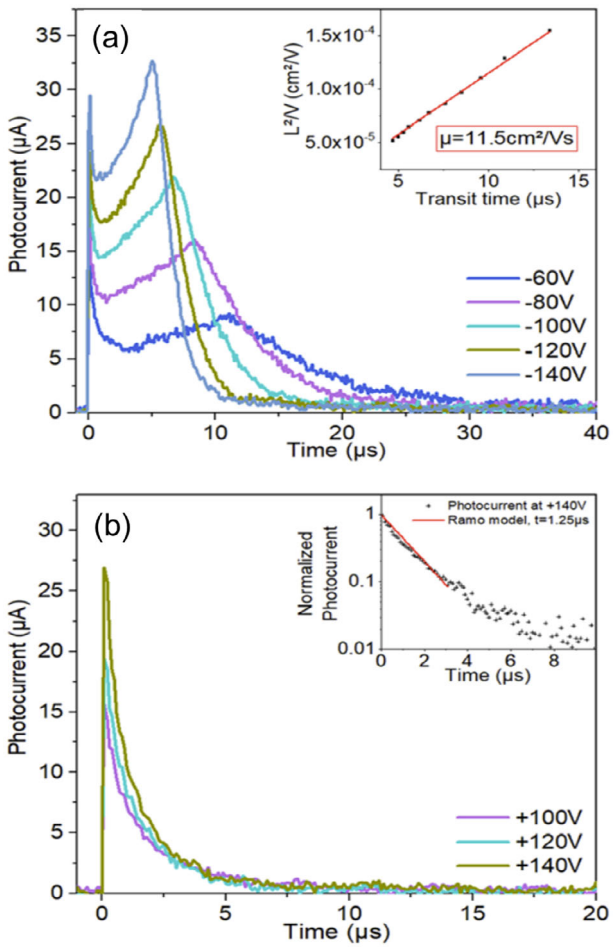


Figure 9. a) TOF hole photocurrent of a MAPbBr3 sample, b) TOF electron photocurrent of a MAPbBr3 sample (inset: photocurrent at +140 V and Ramo model for τ = 1.25 ls).[191]

not increase as the electric field is reduced, being effectively limited by the carrier lifetime. At higher electric field the observed drift time will, in principle, decrease provided that the measurement system is sensitive to shorter drift times and that the mobility of the material is within a reasonable range of values. Such lifetime-limited materials will show an increase in charge amplitude (ie. the integral of the TOF pulse) as a function of increasing electric field due to the increase in carrier drift length with increasing field. Experimentally, a graph of $1/\tau_{tr}$ versus V can be used to determine if a material is lifetime limited, which would show non-linearity at low applied voltages.

The other special case, which is more relevant for perovskite materials, is where the mobility is low. In this case, the carrier drift lengths can be short, despite a high carrier lifetime, if the electric field is low. Therefore, high electric fields are required to fully sweep the carriers across the device thickness. Unlike for lifetime-limited materials, the transit time varies with electric field according to the normal inverse linear relationship in Equation 11 (see Supporting Information). However, since the carriers may not drift across the full device thickness ($\lambda < d$), the measured transit time may give an erroneous value for the drift velocity, i.e., over-estimating the actual mobility value. For thin films this is unlikely to be a significant issue, however for perovskite bulk single crystals a correction may be needed at low field strength due to short carrier drift lengths and limited charge collection efficiency:

$$\mu = \frac{d\lambda}{V\tau_{tr}} \tag{9}$$

4.4. Considerations for Mobility Measured by the Hecht Equation

The Hecht method measures the mean charge amplitude of each pulse as a function of increasing bias, using the Hecht equation to extract the mobility-lifetime product as a direct measure of the charge transport performance of the device (see Supporting Information for detailed description). The general expression that describes the induced current pulse observed at the detector contacts is given by the Shockley-Ramo theorem, which was first applied to radiation detectors to describe the formation of current pulses in gas ionization chambers.[192,193]

However, in the case of low-mobility materials such as organic semiconductors, where the pulse rise times are slow, care is required to use a long pulse shaping time to avoid "ballistic deficit" and loss of signal amplitude. Various factors can complicate the

© 2025 The Author(s). Advanced Functional Materials published by Wiley-VCH GmbH

16163028, 2026, 21, Downloaded from https://advanced.onlinelibrary.wiley.com/doi/10.1002/adfm.202423521 by Adelaide University, Wiley Online Library on [30/09/2026]. See the Terms and Conditions (https://onlinelibrary.wiley.com/terms-and-conditions) on Wiley Online Library for rules of use; OA articles are governed by the applicable Creative Commons License

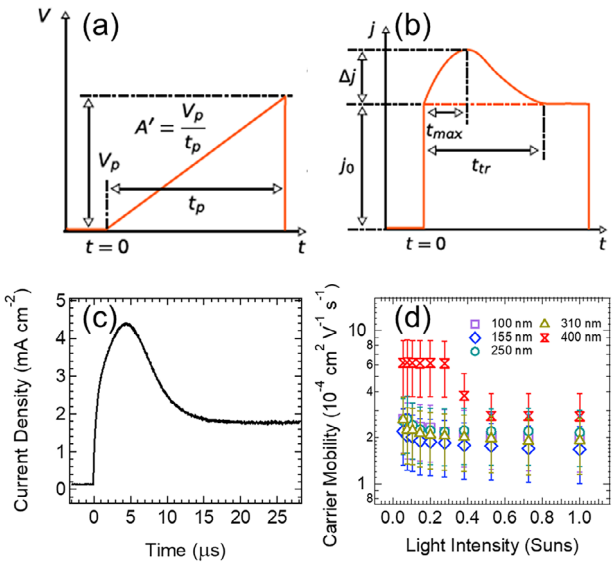


Figure 10. The (a) voltage-time and (c) current-time profiles that are typically obtained from CELIV measurements of devices with photogenerated charges. (c) CELIV current profile, and (d) the computed mobility plotted against changes in the carrier density (light intensity) for radiation detectors fabricated from organic semiconducting donor acceptor pair P3HT:o-IDTBR with thicknesses of 100–500 nm.[26]

Hecht plot analysis, and need to be carefully considered to give an accurate measurement of mobility-lifetime:

(a) Surface Recombination. A potential consequence of the generation of electron-hole pairs close to the detector surface is the effect of surface recombination, which acts as an additional charge loss mechanism in the detector. To describe this effect correctly, an additional surface recombination preterm should be added to the Hecht equation.[194]

(b) Non-uniform Electric Field. In a similar way to TOF analysis, the presence of a non-uniform field depth profile through the device can affect the shape of the Hecht plot. These effects can be described using a modified Hecht equation based on Gunn's theorem, where the field profile is modified by the presence of space charge.[195]

(c) Photocurrent Hecht Measurements. For materials with poor charge transport when signal pulses cannot be observed, the Hecht method can be applied using photocurrent signals, e.g., from a laser or LED. However, the mobility-lifetime products measured from photocurrent data can deviate from the values measured in pulse mode due to the high rate of charge injection from the light source. High rates of charge injection can cause trap filling and the creation of space charge in the material, leading to longer effective lifetimes.

4.5. Considerations for Mobility Measured with Charge Extraction by Linearly Increasing Voltage (CELIV)

CELIV was originally developed as an alternative to TOF to measure charge mobility in microcrystalline silicon (**Figure 10a**),[196] and has since been adapted to determine carrier mobility by analyzing the response of additional charge carriers that are photogenerated by a steady state illumination or by a laser pulse preceding the voltage extraction pulse, a technique known as photo-CELIV (Figure 10b).[197]

The CELIV measurement is primarily a bulk generation, thin film measurement technique where charge generation and spatial distribution prior to applying the extraction pulse is assumed to be uniform throughout the film (see details in Supporting Information). Therefore, charge mobility in thin film samples down to 100 nm can be measured. This makes CELIV a particularly useful tool for probing the mobility in operational devices fabricated from disordered organic semiconductors, where film thicknesses are typically limited to several hundred nanometers. Figure 10c, d show typical current traces and extracted mobility data for organic photodiodes used as radiation detectors, demonstrating a thickness and light-intensity independent mobility value up to detector thicknesses of 310 nm, beyond which the technique produces incorrect data due to incomplete charge extraction.

A limitation of the CELIV technique is that the sign of the charge carriers cannot be directly determined in such "bulk" measurements. Additional complications arise when electron and hole mobilities are asymmetric,[198] if recombination of the photogenerated charges takes place during charge extraction,[199] or if the charge distribution is not uniform.[200] The latter may occur as a consequence of charge carrier redistribution during the delay time between the laser pulse and the application of the charge extraction voltage ramp. A more refined method for probing the mobility and lifetime of photogenerated charge carriers in organic photodiodes under real operating conditions is to apply a time-dependent pre-extraction compensating voltage pulse representing the voltage-decay profile of the sample, called the OTRACE method.[201] Alternatively, a fast (nanosecond) switch can be employed in the measurement circuit to keep the device at a high impedance (open circuit) during the delay time and switch to low impedance simultaneously with the application of the charge extraction time.[200]

The CELIV technique has also been further developed by measuring the charge mobility of injected charge carriers.[202] Therefore, CELIV now represents a whole suite of charge extraction techniques suitable for exploring various device geometries and scientific/technical needs.[203–205] However, the availability of these various protocols and refinements does represent an increased level of complexity and enhances the possibility of incorrect application and analysis. Comparative mobility and lifetime studies already existing between CELIV, TOF, impedance, and fully optical transient absorption-based charge carrier lifetime measurements on the same materials and architectures can provide a practical guide to assess the cross-measurement usefulness of the measured values.[199]

5. Radiation Hardness as a Key Metrics for Organic Semiconductor and Perovskite Radiation Detectors

Organic and perovskite materials are attractive for a range of medical, personal dosimetry, and space applications. However, a significant proportion of the current research on these materials is directed at imaging applications with little or no attention directed to the radiation hardness characterization required for

© 2025 The Author(s). Advanced Functional Materials published by Wiley-VCH GmbH

16163028, 2026, 21, Downloaded from https://advanced.onlinelibrary.wiley.com/doi/10.1002/adfm.202423521 by Adelaide University, Wiley Online Library on [30/09/2026]. See the Terms and Conditions (https://onlinelibrary.wiley.com/terms-and-conditions) on Wiley Online Library for rules of use; OA articles are governed by the applicable Creative Commons License

applications in harsher radiation conditions due to the low dose typically delivered during irradiation for diagnostic purposes. On the other hand, radiology and space applications are identified as critical environments where the requirements of radiation hardness in materials and detectors are tighter and must satisfy stringent specifications. Prolonged exposure to ionizing radiation will cause chemical and structural damage to a material. The total ionizing dose (TID) may change the electrical transport properties of the detector, altering the detection performance. Another parameter that is critical for a radiation detector is the dark current or baseline stability with accumulated dose. The parameter used for characterization leakage current in radiation detectors is called Radiation Induced Leakage Current (RILC) or radiation damage rate and is calculated as the linear increase of leakage current at a fixed bias as a function of the irradiation fluence or dose.[206] Therefore, it is imperative that the effects of radiation damage are reported, and perhaps more importantly, comprehensively understood at a mechanistic level for emerging organic semiconductor and perovskite materials. Since TID levels and type of radiation will vary for typical applications, a proposed pathway toward reporting radiation hardness is to determine the radiation stability (sensitivity and baseline) as a function of both the total irradiation time and the duty cycle of radiation employed for data collection (indicating the performance stability) and a predictive indicator of stability across repetitive irradiation cycles (indicating the lifetime stability).

Intrinsically, ionization and atomic displacement within a detector material produce damage to the molecular structure. Furthermore, unlike the generation of electronic charges with visible light, where one absorbed photon generates one charge carrier, absorption of a single high-energy photon or charged particle generates several charge carriers, proportional to the energy deposited in the interaction processes. Therefore, the photodegradation mechanisms induced by light that have been heavily studied for perovskites and organic semiconductors are not likely to be directly comparable to their application in ionizing radiation detectors.[207] For instance, polymeric and small-molecule organic semiconductor materials are known to undergo changes in interchain bonding and local energetic disorder when exposed to prolonged ionizing radiation, whereas perovskites, being ionic crystals, experience ion migration and crystalline fracture when generating ionized charge inside the material unless extracted quickly (**Figure 11**). Extrinsically, the beam properties are also important. For instance, in two beams with identical photon or particle fluxes, the beam with the lowest energy will increase the probability of interaction with the detector active layer via the photoelectric effect. This will promote a higher dose absorption in comparison to the beam with the highest energy, where Compton scattering is dominant and less energy will be absorbed by the detector. However, this effect could be counterbalanced by the capability of high-energy particles to create atomic interactions, generating spallation and fragmentation within the substrate, altering the molecular or crystalline structure, and so altering the pristine electronic or ionic transport performances.

Considering the critical role of radiation hardness in developing the next generation of radiation detector materials, measuring, interpreting, and reporting radiation stability results in a manner that enables direct comparisons between different laboratories, materials, and applications is becoming increasingly important. In this work, we have classified a collection of results reported in literature based on the type of irradiating particle for both perovskite and organic semiconductors, seeking to draw out a consensus on the reporting of metrics for radiation hardness. A more extensive overview of specific radiation hardness results can be found in recent comprehensive reviews for organic semiconductors[10] and perovskite materials.[208,209]

5.1. Radiation Hardness for Photons

Photons are abundant in space environments and medical applications. Cosmic events and features emit a wide range of photon energies (from eV to MeV) with a flux that varies from 10^{-1} photons m^{-2} s^{-1} (10 MeV) to 10^{8} photons m^{-2} s^{-1} (1 keV),[210] while imaging and radiology applications span energies for from keV to tens of MeV at a photon flux of 10^{13} photons m^{-2} s^{-1}.[211] The standard source for characterization of photon-induced total dose damage is Cobalt-60 (Co-60), a 1.2 MeV monochromatic source with dose rates from ≈10 mGy h^{-1} for laboratory sources to 1–5 kGy h^{-1} for specialized sources at high-end facilities. Such specialized sources can utilize very high dose rates to provide accelerated testing of materials and devices, thus estimating radiation effects across a functional lifetime from a narrow time window of testing.[212,213] Another common source used for radiation stability testing is Cesium-137 (^{137}Cs) irradiators, which produce gamma rays with an energy of 662 keV and low dose rates (up to 15–20 Gy h^{-1}).[214,215] Co-60 is recommended by military and space qualification standards for accelerated radiation damage characterization due to the high penetration of the gamma rays and production of a whole range of interactions, including Compton scattering and pair-production. Co-60 also produces gamma photons with energy comparable to the average energy of x-ray photon beams produced with a 6 MV accelerating voltage from medical linear accelerators, making it convenient for accelerated testing and calibration of medical instrumentation. For space applications, the benchmark of anticipated total dose across a device lifetime is 1–10 kGy for middle to low Earth orbits,[216] while in medical applications, a device designed for quality assurance must be able to cope with irradiation doses of 30–40 kGy for a shelf life of 7 to 10 years.[217] Since both the pathways and the kinetics of radiation-induced degradation depend on the type of radiation, dose rate, and total accumulated dose, it is strongly recommended that the appropriate radiation source and total doses are applied to devices depending on their application when determining the radiation hardness of new materials and/or device architectures.

Radiation damage in organic and perovskite semiconductors due to exposure to photons is often reported to induce a strong decrease in the photon-to-electrical conversion efficiency (PCE) and the photocurrent during the initial part of the irradiation.[218–221] Studies exploring the effect of high energy photons on the radiation hardness of semiconducting polymers and perovskites typically focus on structure-function properties, utilizing measurements of the material's intrinsic properties such as shifts in the electrical characteristics of the highest occupied molecular orbital (HOMO) and lowest unccupied molecular orbitals (LUMO) energy levels or charge carrier dynamics in semiconducting polymer films. Early studies revealed a typical decrease

© 2025 The Author(s). Advanced Functional Materials published by Wiley-VCH GmbH

16163028, 2026, 21, Downloaded from https://advanced.onlinelibrary.wiley.com/doi/10.1002/adfm.202423521 by Adelaide University, Wiley Online Library on [30/09/2026]. See the Terms and Conditions (https://onlinelibrary.wiley.com/terms-and-conditions) on Wiley Online Library for rules of use; OA articles are governed by the applicable Creative Commons License

16163028, 2026, 21, Downloaded from https://advanced.onlinelibrary.wiley.com/doi/10.1002/adfm.202423521 by Adelaide University, Wiley Online Library on [30/09/2026]. See the Terms and Conditions (https://onlinelibrary.wiley.com/terms-and-conditions) on Wiley Online Library for rules of use; OA articles are governed by the applicable Creative Commons License

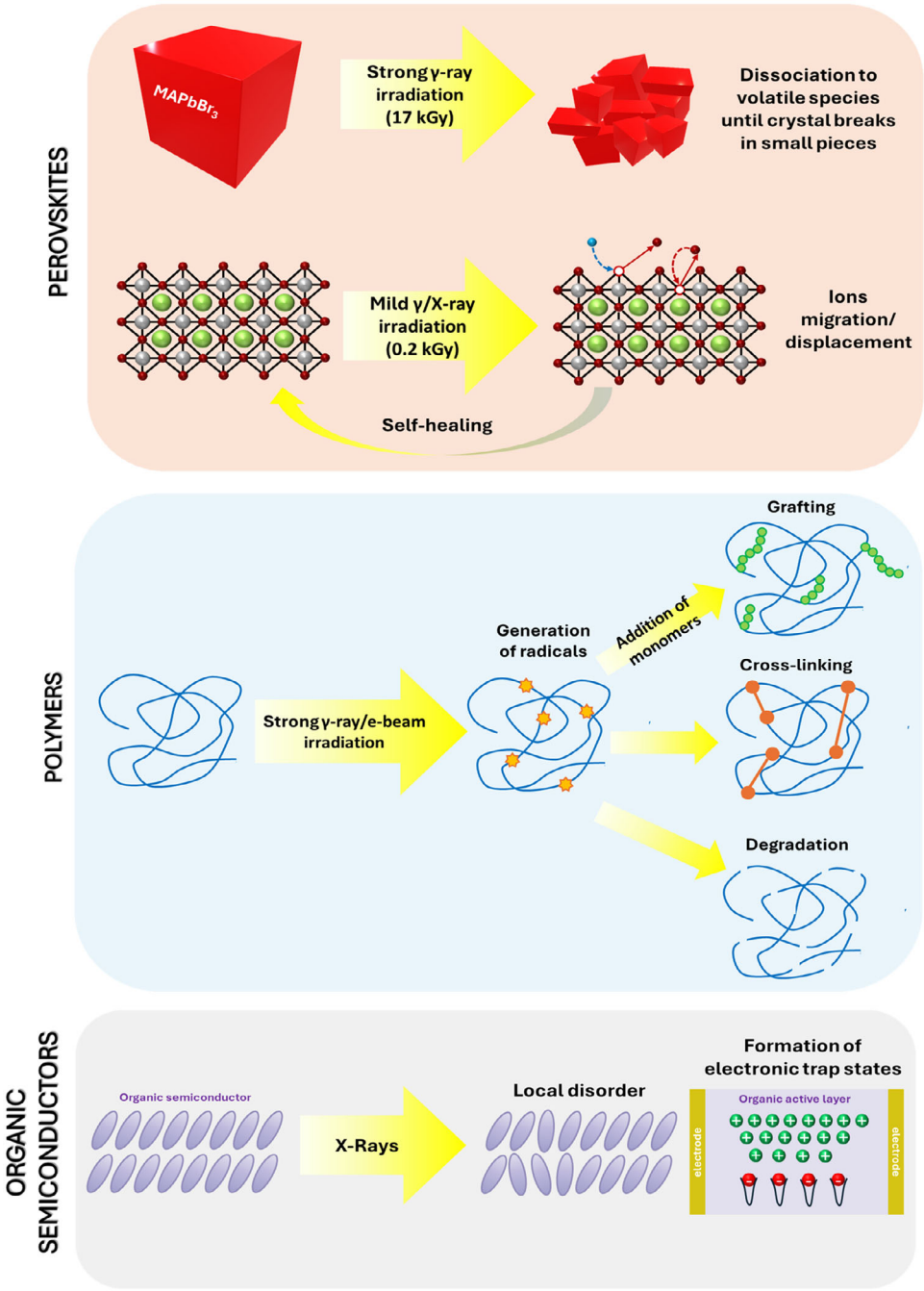


Figure 11. An illustration of the impact of prolonged ionizing radiation exposure on the structure of perovskites (top), polymers (middle), and small molecule organic semiconductors (bottom), showing the main mechanisms resulting in a loss of radiation hardness.

in the performance of photodiodes fabricated with organic polymers and perovskites.[91,221–224] As studies became more sophisticated, specific mechanisms were able to be elucidated. These studies highlighted that defect creation due to polymer bond or perovskite lattice distortions was the predominant form of degradation due to ionizing radiation.[26,221] Careful selection of multi-stack materials that combine radiation tolerant polymers and perovskites have recently been shown to have outstanding radiation tolerance,[225] with almost negligible degradation in performance of the photoactive materials after 23 kGy of accumulated dose from a Cs-137 source of a polytetraarylamine (PTAA)/perovskite stack structure fabricated on indium doped tin oxide (ITO) glass. Further studies showed that radiation damage by gamma rays affects the different materials in multi-stack photodiodes very differently, with a combination of tri-cation perovskite active layer and semiconducting polymer transport layers irradiated with Co-60 gamma rays showing a strong effect localized to just the phenyl-C61-butyric acid methyl ester (PCBM) layer.[226] These

 © 2025 The Author(s). Advanced Functional Materials published by Wiley-VCH GmbH

types of effects are confirmed by the studies of Large et al., where the performance of polymer devices with different electron acceptors were measured before and after 10 kGy irradiation with Co-60 gamma rays for bulk heterojunction photodiodes, concluding that planar non-fullerene acceptors had a much greater tolerance to ionizing radiation than the fullerene derivative PCBM.[207] It has also been shown that the substrates and packaging materials themselves can be radioluminescent, and thus effect the sensitivity of devices.[227,228] It follows that the substrates and packaging should then also be considered in radiation hardness studies. These results suggest it is important to try and measure multiple devices with varying stack layer structure to isolate the effects of each material in the multi-layer photodiode independently where possible.

However, further complicating analysis of the radiation stability of new materials is that semiconducting polymers and perovskite materials have both demonstrated an ability to "self-anneal" or "self-heal", where the performance of the materials spontaneously recovers either partially or fully following removal of the radiation beam.[229–232] Thus, it is critical when determining the radiation stability to clearly specify the temporal history of the performance measurements. Ideally for reproducible and comparable radiation hardness determinations in different laboratories, performance metrics would be taken immediately prior to radiation exposure, immediately following radiation exposure (or for materials with a strong transient response, at some clearly reported time where a reliable steady state response is obtained), and then at a predetermined time after the removal of exposure to capture a full picture of the complex radiation hardness properties of novel semiconducting materials.

5.2. Radiation Hardness for Electrons

Electrons represent the most common high-energy particle present in medical applications, either as a primary source or as a secondary particle generated by Compton scattering or direct ionization from primary photons. The role of high-energy electrons has been shown to damage the C-H or C-C bonds of conjugated polymers and perovskites, producing a combination of point defect, cross-linking, and chain scission effects that impede charge carrier transport and produce recombination centers of minority carriers and trap centers for majority carriers.[233–235] These processes will deteriorate the charge collection efficiency, in the form of a reduced PCE or short circuit photocurrent density of the sensitive layer. The production of dangling bonds will also create new generation and recombination centers, which will increase the dark current and compromise the baseline stability. However, the typically very thin (50–500 nm) layer of the sensitive volume in polymer and perovskite radiation detectors makes these kinds of devices intrinsically very radiation hard to electrons, often more so than devices fabricated from their crystalline semiconductor counterparts.[236,237]

Interaction of electrons with the device substrates and encapsulation materials is also a crucial parameter in the overall radiation hardness of devices. Glass substrates have been reported to become darkened by 1 MeV electrons with fluences below 10^{14} p/cm^2,[238] a flux at which there is little observed effect on morphology and crystal phase in perovskite materials[239,240] Other recent work suggests that radiation damage by electrons is dominated by heating-induced defects and structural phase transformations.[241]

5.3. Radiation Hardness for Protons

Sensors developed for interplanetary space exploration or hadron therapy will be exposed to high fluxes of energetic protons across their working lifetime (10^4 – 10^6 protons m^{-2} s^{-1} for space, 10^8 – 10^{11} protons m^{-2} s^{-1} for hadron therapy).[242,243] These devices will require a characterization of the variation of the responsiveness in the form of PCE or radiation-induced current as a function of irradiation by protons with energies from 1–300 MeV.[244,245] High-energy protons can cause severe damage to organic and perovskite devices if their residual energy at the impact with the device is in the order of 1 MeV or less. The exponential increase of the Linear Energy Transfer (LET) as the particle reduces its speed produces displacement damage due to the elastic impact of the proton with the substrate atoms. This results in a highly dense ionization track along the proton path which may trigger hydrogen atom displacement and interstitial iodine atoms responsible for strong deterioration of carrier transport.[246] Neitzert et al. reported a characterization of $CH_3NH_3PbI_3$ perovskite solar cell degradation after irradiation with 68 MeV protons, where the photocurrent and PCE were reduced by a factor of 20–30% after exposure to a proton beam with a fluence of 10^{12} cm^{-2}.[247] Both the particle fluence and energy reported in this work are relevant for both space and medical applications (such as ocular melanoma proton therapy). The fluence of 10^{12} cm^{-2} corresponds to approximately three years in deep space missions or ≈70 Gy as a total absorbed dose in water, corresponding to two patient therapy protocols at the recommended prescribed total dose for hadron therapy (i.e., the sum of fractionated doses received across multiple treatments that comprise hadron therapy).[248] These conversions reveal that developing sensors for medical applications should explore longer radiation hardness characterization procedures than those developed for space applications. A thorough radiation hardness characterization should also explore effects from a wider range of energies since the electronic stopping power, and therefore the LET, is the function of the proton energy. Lower energies (e.g, commonly employed 10, 20, and 68 MeV) can reflect proton energy distribution well for space applications, however, these energies are too limited for medical applications, which should include energies in the range of 70 – 250 MeV, commonly adopted for prostate cancer proton therapies. In particular, the latter energy range presents a unique opportunity for emerging organic and perovskite semiconducting materials due to their suitability for satisfying both requirements of detectors in therapy applications (flexible, large area, and low power detectors for real-time dosimetry with a response that is equivalent to biological tissue without complex calibrations). There are currently very limited experimental studies of radiation damage characterization for organic or perovskite devices at these energy ranges, however, there are over 100 active proton therapy centers in the world and a further 60 under development,[249] highlighting an urgent need for new materials that can accurately monitor the dose of high energy protons in a controlled and calibrated fashion.

© 2025 The Author(s). Advanced Functional Materials published by Wiley-VCH GmbH

16163028, 2026, 21, Downloaded from https://advanced.onlinelibrary.wiley.com/doi/10.1002/adfm.202423521 by Adelaide University, Wiley Online Library on [30/09/2026]. See the Terms and Conditions (https://onlinelibrary.wiley.com/terms-and-conditions) on Wiley Online Library for rules of use; OA articles are governed by the applicable Creative Commons License

6. Imaging Metrics for Organic Semiconductor and Perovskite Radiation Detectors

One of the most frequent applications for radiation detection is imaging. Whilst the focus of radiation imaging is often on the medical arena, given the significant advancements in methods of disease diagnosis and treatment enabled by technological advances in ionizing radiation detectors,[250] radiation imaging is also critical in security screening and industrial quality insurance.[251,252] The evaluation of image quality typically requires quantitative parameters, although given the multiple factors upon which image quality depends, comparing images obtained across multiple systems can get complicated.[253,254] At a high level, image transfer theory has been widely used in the field to guide this process. In a generic form, the input signal f (x, y) Equation (10) is transformed by the detector into an output signal g(x, y), where the system operator S represents the detector effect on the input signal:[2]

$$g(x,y) = S\left[f(x,y)\right] \tag{10}$$

The system operator S characterizes the detector used the produce the imaging signal. In general, the quality of images acquired using ionizing radiation can be analyzed from the detector perspective by considering three key components: 1) factors impacting imaging contrast, 2) factors affecting spatial resolution, and 3) sources of image noise.[255] Whilst these properties are often inter-related and can be influenced by all aspects of the image-forming process (e.g., the source properties, the source–object arrangement, and the performance of the detector, a good starting point to assess the performance of radiation detectors for imaging is to determine their performance across the above three criteria.

6.1. Contrast

Production of an image requires differential attenuation of a radiation beam as it passes through different parts of an object. The native contrast produced from differences in signal brightness due to differing attenuation of radiation at a set energy spectrum and angle between an object of interest and its surroundings is known as intrinsic contrast. Whilst often noted as a key metric for image quality, it is ideally independent of the detector and relies purely upon it, and thus is unsuitable as a performance metric for new detector systems.[255] However, for polychromatic sources, this native image contrast is impacted by the differing attenuation of the detector material at different energies, and it thus changes both the number of photons being detected and the effective energy spectrum producing the image, both of which alter contrast.

Distinguishing intrinsic contrast from the additional effects of the detector can be difficult from a characterization perspective. To provide insight into the effect of the detector, the concept of the limit of detection can be useful. This parameter measures the lowest detectable dose that can be employed to obtain a distinguishable image, and is defined by the International Union of Pure and Applied Chemistry (IUPAC) as the equivalent dose rate required to produce a signal greater than three times the noise level (signal-to-noise ratio, SNR = 3).[256] However, since the SNR is a statistical parameter, it could be possible to obtain superior imaging at a set SNR by acquiring the image over a longer time period to boost photon statistics. Thus, we suggest that an accompanying metric to the limit of detection, if reporting this value as a projection of data beyond the actual range of values measured, is to report the combination of the SNR and time taken to acquire the actual image that is being shown as data in any study.

6.2. Spatial Resolution

Spatial resolution refers to an imaging system's ability to distinguish adjacent structures as separate from each other.[257] As for the imaging contrast discussed in Section 6.1, there are several components of the imaging process that influence spatial resolution that are independent of the detector (source sharpness, object scatter, collimators, etc), which fall beyond the scope of this Perspective. Here we focus on quantitatively capturing the features of organic semiconducting and perovskite radiation detectors which influence the spatial resolution of an image, a feature which can only be characterized when detectors are fabricated into pixellated arrays. Thus, the first important metric to report for spatial resolution determination is the pixel pitch, which is the distance from the center of one pixel to the center of the neighboring pixel.

Whilst there are many features of a detector than can influence spatial resolution (optical cross talk for isotropic scintillator emission, detector scatter, electrical cross-talk between pixels), one metric frequently used to quantify the combination of these effects is the modulation transfer function (MTF), which describes the detectors' ability to transfer the input signal modulation of a given spatial frequency in relation to its output.[99] Imagining a standard line pattern containing materials which alternate between equally spaced bars of opaque and transparent materials can be used to determine the spatial resolution, which is typically reported in units of line pairs per millimetre (lp per mm) for radiation detectors.[106] If the device used to determine the spatial resolution contains a sharp attenuating edge, the MTF can be directly computed from the image of the test pattern.[258] The metric for quantitative comparison of the spatial resolution we suggest for organic semiconducting and perovskite radiation detecting systems is the same as that used to currently compare inorganic systems in radiography applications, namely the spatial frequency of a test pattern in lp per mm at which the MTF of the imaging system drops to 0.2.

6.3. Signal to Noise Ratio

The signal-to-noise ratio (SNR) is an important metric that combines the effects of contrast, resolution, and noise.[257] Whilst a simple determinant of SNR is the photocurrent measured by the detector with the radiation beam on compared to the noise current (standard deviation of the photocurrent), a more sophisticated measure of the signal-to-noise performance of a detector

© 2025 The Author(s). Advanced Functional Materials published by Wiley-VCH GmbH

16163028, 2026, 21, Downloaded from https://advanced.onlinelibrary.wiley.com/doi/10.1002/adfm.202423521 by Adelaide University, Wiley Online Library on [30/09/2026]. See the Terms and Conditions (https://onlinelibrary.wiley.com/terms-and-conditions) on Wiley Online Library for rules of use; OA articles are governed by the applicable Creative Commons License

is the detector quantum efficiency (DQE).[259] The DQE can be defined by Equation (11):[260]

$$DQE\ \ (f) = \frac{qG^2 MTF(f)^2}{NPS\,(f)} \tag{11}$$

where q is the average number of photons incident onto the detector per unit area, and G is the gain factor (see Section 3.1.3), and MTF(*f*) is the modulation transfer function (see Section 6.2). NPS(*f*) is the output noise power spectrum, which measures the magnitude of noise and its dependence on spatial frequencies. The detector NPS can be obtained by taking the discrete Fourier transform (DFT) of the auto-covariance of the counts measured by the detector array.[261]

7. Recommendations for Reporting Performance Metrics in Radiation Detectors

The above discussions have revealed the lack of standard approaches for testing and reporting the performance of novel perovskite and organic semiconductor materials and device architectures for radiation detection. To address this absence of standardization, we have presented here an overview of factors affecting the variation in common performance metrics and provided a recommendation for key metrics to report to help standardize the characterization of radiation detectors fabricated with next-generation semiconductors. For each metric, we identified associated critical experimental parameters and procedures that could be reported to improve reproducibility and consistency (Figure 2). These recommendations include:

- *Details of the Ionizing Radiation Source*
  The interactions of detector materials and devices are strongly influenced by the radiation source used to characterize the performance. To allow comparisons between studies with different sources, it is recommended that the following details be reported:
  - The energy of the radiation itself, or for broad spectrum beams, the accelerating voltage used to produce the radiation.
  - The dose rate of the radiation,
  - The spectrum of the ionizing radiation, which could be provided via direct data or by reporting the target source producing the radiation (which have known spectra that can be retrieved from databases). It is also recommended that reports specify whether the source is outputting monochromatic or Bremsstrahlung radiation, and any filters used to modify the radiation beam properties.
- *Device Sensitivity*
  As a key metric for detector performance, sensitivity is a critical measure used to compare different materials and device architectures. It is recommended that the following details be reported when characterizing the detector sensitivity:
  - The range of radiation energies across which the sensitivity was measured, and a statement indicating the linearity of the sensitivity within this energy range.
  - The dependence of the sensitivity on the radiation dose rate.
  - Sufficient data to determine the photoconductive gain of the device being measured. This could be provided either via direct measurement of relevant parameters (see Section 3.1.3) or by comparing the measured sensitivity to the estimated theoretical maximum sensitivity value.
- *Charge Carrier Mobility*
  The method used to measure this parameter can strongly influence the value obtained. To aid with consistency in comparisons across studies where mobility is a key figure of merit, it is recommended that:
  - The field dependence of mobility values is reported.
  - The dependence of mobility on the active layer thicknesses of devices is reported.
- *Radiation Hardness*
  Studies can vary widely in the process employed to characterize radiation hardness. To facilitate accurate comparisons between studies where radiation stability is a key metric, it is recommended that:
  - The total ionizing radiation dose is reported, including details on the number of radiation exposures and the duty cycle for repetitive testing.
  - The radiation-induced leakage current (radiation damage rate) is reported.
- *Imaging*
  Numerous factors can influence the quality of an image obtained using an ionizing radiation source. To enable the most precise comparisons between studies with different detectors, it is recommended that:
  - The detection limit, or a combination of the detector SNR and acquisition time used to acquire an image, is reported.
  - The spatial resolution of a test pattern (in lp per mm) at which the modulation transfer function drops to 0.2 is noted.
  - The detective quantum efficiency is measured and reported.

8. Conclusion

In this Perspective, we have presented an overview of the difficulty in capturing the performance of organic and perovskite materials for radiation detection using characterization procedures designed for inorganic technologies. We discuss the properties of organic semiconductors, metal halide perovskites and organic–inorganic hybrid materials and devices that can uniquely influence typical performance metrics, highlighting how comparisons of innovations in materials and device architectures should be carefully considered when making determinations regarding critical advancements in the field. We have highlighted that, unlike approaches in other fields such as photovoltaics research, where materials and devices are characterized and reported using stringently reviewed standard protocols, radiation detectors fabricated from organic semiconductors and perovskite materials are currently measured under highly variable conditions using a wide variety of approaches. Accordingly, it has become increasingly difficult to directly compare the performances reported by different groups and to elucidate whether innovations are inherent to the next-gen materials being utilized or result from more macroscale device architecture features. We present our perspective on improving standardization in experimental characterization and reporting as the field of organic semiconducting and perovskite radiation detection continues to evolve. This process involves a recommendation for three key metrics

© 2025 The Author(s). Advanced Functional Materials published by Wiley-VCH GmbH

16163028, 2026, 21, Downloaded from https://advanced.onlinelibrary.wiley.com/doi/10.1002/adfm.202423521 by Adelaide University, Wiley Online Library on [30/09/2026]. See the Terms and Conditions (https://onlinelibrary.wiley.com/terms-and-conditions) on Wiley Online Library for rules of use; OA articles are governed by the applicable Creative Commons License

(sensitivity, mobility/lifetime, and radiation hardness) to report, with accompanying critical experimental parameters and procedures identified for inclusion in publications in order to improve reproducibility and consistency. We hope that the considerations for conducting and reporting radiation detection studies on organic semiconducting and perovskite materials and devices outlined here will improve comparisons between data from different laboratories and from different device architectures (Supporting Information).

Supporting Information

Supporting Information is available from the Wiley Online Library or from the author.

Acknowledgements

The authors acknowledge the facilities, and the scientific and technical assistance of Microscopy Australia at the University of South Australia, a facility that is co-funded by the University of South Australia, the State and Federal Governments. This work was supported by grants from the Office of National Intelligence (NIPG grant scheme), Australian Research Council (DP230102705 and FT230100154) and National Health and Medical research Council (Ideas Scheme; 2003775).

Conflict of Interest

The authors declare no conflict of interest.

Keywords

mobility, organic semiconductors, perovskites, polymer, printed electronics, radiation detection, sensitivity, X-ray

Received: December 1, 2024
Revised: March 8, 2025
Published online: May 13, 2025

[1] S. Dhanekar, K. Rangra, *Adv. Mater. Technol.* **2021**, *6*, 2000895.
[2] J. Seco, B. Clasie, M. Partridge, *Phys. Med. Biol.* **2014**, *59*, R303.
[3] L. Narici, T. Berger, D. Matthia, G. Reitz, *Front. Oncol.* **2015**, *5*, 273.
[4] M. D. Alam, S. S. Nasim, S. Hasan, *Prog. Nucl. Energy* **2021**, *140*, 103918.
[5] M. Menichelli, L. Servoli, N. Wyrsch, *Front. Phys.* **2022**, *10*, 1.
[6] P. Rehak, *IEEE Trans. Nucl. Sci.* **2004**, *51*, 2492.
[7] V. Dědič, J. Zázvorka, M. Rejhon, J. Franc, R. Grill, P. J. Sellin, *J. Appl. Phys.* **2014**, *116*, 053702.
[8] M. Ohmori, Y. Iwase, R. Ohno, *Mater. Sci. Eng. B* **1993**, *16*, 283.
[9] A. M. Zeidell, T. Ren, D. S. Filston, H. F. Iqbal, E. Holland, J. D. Bourland, J. E. Anthony, O. D. Jurchescu, *Adv. Sci.* **2020**, *7*, 2001522.
[10] J. A. Posar, M. Petasecca, M. J. Griffith, *Flex. Printed Electron.* **2021**, *6*, 043005.
[11] O. D. I. Moseley, T. A. S. Doherty, R. Parmee, M. Anaya, S. D. Stranks, *J Mater Chem C Mater* **2021**, *9*, 11588.
[12] X. He, Y. Deng, D. Ouyang, N. Zhang, J. Wang, A. A. Murthy, I. Spanopoulos, S. M. Islam, Q. Tu, G. Xing, Y. Li, V. P. Dravid, T. Zhai, *Chem. Rev.* **2023**, *123*, 1207.
[13] M. Chen, C. Wang, W. Hu, *J. Mater. Chem. C* **2021**, *9*, 4709.
[14] L. Basiricò, A. Ciavatti, B. Fraboni, *Adv. Mater. Technol.* **2020**, *6*, 2000475.
[15] Y. Y. Kim, T. Y. Yang, R. Suhonen, A. Kemppainen, K. Hwang, N. J. Jeon, J. Seo, *Nat. Commun.* **2020**, *11*, 5146.
[16] M. J. Griffith, N. P. Holmes, D. C. Elkington, S. Cottam, J. Stamenkovic, A. L. D. Kilcoyne, T. R. Andersen, *Nanotechnology* **2020**, *31*, 092002.
[17] M. J. Griffith, N. A. Cooling, B. Vaughan, D. C. Elkington, A. S. Hart, A. G. Lyons, S. Quereshi, W. J. Belcher, P. C. Dastoor, *IEEE J. Selected Topics Quant. Electron.* **2016**, *22*, 112.
[18] A. Y. Al-Ahmad, F. Almayhi, M. F. Al-Mudhaffer, M. J. Griffith, W. Liu, S. Li, K. Sivunova, D. Elkington, N. A. Cooling, K. Feron, M. Shi, W. Belcher, H. Chen, P. Dastoor, T. R. Andersen, *Sustain. Energy Fuels* **2020**, *4*, 940.
[19] A. Dey, J. Ye, A. De, E. Debroye, S. K. Ha, E. Bladt, A. S. Kshirsagar, Z. Wang, J. Yin, Y. Wang, L. N. Quan, F. Yan, M. Gao, X. Li, J. Shamsi, T. Debnath, M. Cao, M. A. Scheel, S. Kumar, J. A. Steele, M. Gerhard, L. Chouhan, K. Xu, X. G. Wu, Y. Li, Y. Zhang, A. Dutta, C. Han, I. Vincon, A. L. Rogach, et al., *ACS Nano* **2021**, *15*, 10775.
[20] R. L. Z. Hoye, J. Hidalgo, R. A. Jagt, J. P. Correa-Baena, T. Fix, J. L. MacManus-Driscoll, *Adv. Energy Mater.* **2021**, *12*, 2100499.
[21] J. Jeong, M. Kim, J. Seo, H. Lu, P. Ahlawat, A. Mishra, Y. Yang, M. A. Hope, F. T. Eickemeyer, M. Kim, Y. J. Yoon, I. W. Choi, B. P. Darwich, S. J. Choi, Y. Jo, J. H. Lee, B. Walker, S. M. Zakeeruddin, L. Emsley, U. Rothlisberger, A. Hagfeldt, D. S. Kim, M. Gratzel, J. Y. Kim, *Nature* **2021**, *592*, 381.
[22] A. Ciavatti, R. Sorrentino, L. Basiricò, B. Passarella, M. Caironi, A. Petrozza, B. Fraboni, *Adv. Funct. Mater.* **2021**, *31*, 2009072.
[23] M. J. Griffith, S. Cottam, J. Stamenkovic, J. A. Posar, M. Petasecca, *Front. Phys.* **2020**, *8*, 1.
[24] F. A. Boroumand, M. Zhu, A. B. Dalton, J. L. Keddie, P. J. Sellin, J. J. Gutierrez, *Appl. Phys. Lett.* **2007**, *91*, 033509.
[25] H. M. Thirimanne, K. Jayawardena, A. J. Parnell, R. M. I. Bandara, A. Karalasingam, S. Pani, J. E. Huerdler, D. G. Lidzey, S. F. Tedde, A. Nisbet, C. A. Mills, S. R. P. Silva, *Nat. Commun.* **2018**, *9*, 2926.
[26] J. A. Posar, J. Davis, S. Alnaghy, D. Wilkinson, S. Cottam, D. M. Lee, K. L. Thompson, N. P. Holmes, M. Barr, A. Fahy, N. C. Nicolaidis, F. Louie, B. Fraboni, P. J. Sellin, M. L. F. Lerch, A. B. Rosenfeld, M. Petasecca, M. J. Griffith, *Adv. Mater. Technol.* **2021**, *6*, 2001298.
[27] J. A. Posar, J. Davis, M. J. Large, L. Basirico, A. Ciavatti, B. Fraboni, O. Dhez, D. Wilkinson, P. J. Sellin, M. J. Griffith, M. L. F. Lerch, A. Rosenfeld, M. Petasecca, *Med. Phys.* **2020**, *47*, 3658.
[28] K. R. Dudipala, T. H. Le, W. Nie, R. L. Z. Hoye, *Adv. Mater.* **2024**, *36*, 2304523.
[29] O. P. Dimitriev, *Chem. Rev.* **2022**, *122*, 8487.
[30] Y. Kanemitsu, T. Handa, *Japan. J. Appl. Phys.* **2018**, *57*, 090101.
[31] W. Xiang, S. Liu, W. Tress, *Energy Environ. Sci.* **2021**, *14*, 2090.
[32] M. V. Khenkin, E. A. Katz, A. Abate, G. Bardizza, J. J. Berry, C. Brabec, F. Brunetti, V. Bulović, Q. Burlingame, A. Di Carlo, R. Cheacharoen, Y.-B. Cheng, A. Colsmann, S. Cros, K. Domanski, M. Dusza, C. J. Fell, S. R. Forrest, Y. Galagan, D. Di Girolamo, M. Grätzel, A. Hagfeldt, E. von Hauff, H. Hoppe, J. Kettle, H. Köbler, M. S. Leite, S. Liu, Y.-L. Loo, J. M. Luther, et al., *Nat. Energy* **2020**, *5*, 35.
[33] L. Pan, S. Shrestha, N. Taylor, W. Nie, L. R. Cao, *Nat. Commun.* **2021**, *12*, 5258.
[34] S. Wu, C. Liang, J. Zhang, Z. Wu, X. L. Wang, R. Zhou, Y. Wang, S. Wang, D. S. Li, T. Wu, *Angew. Chem.* **2020**, *132*, 18764.
[35] G. Bratina, E. Pavlica, *Org. Electron.* **2019**, *64*, 117.
[36] Z. Xu, X. Liu, Y. Li, X. Liu, T. Yang, C. Ji, S. Han, Y. Xu, J. Luo, Z. Sun, *Angew. Chem. Int. Ed. Engl.* **2019**, *58*, 15757.
[37] J. Ferrer Orri, T. A. S. Doherty, D. Johnstone, S. M. Collins, H. Simons, P. A. Midgley, C. Ducati, S. D. Stranks, *Adv. Mater.* **2022**, *34*, 2200383.

© 2025 The Author(s). Advanced Functional Materials published by Wiley-VCH GmbH

16163028, 2026, 21, Downloaded from https://advanced.onlinelibrary.wiley.com/doi/10.1002/adfm.202423521 by Adelaide University, Wiley Online Library on [30/09/2026]. See the Terms and Conditions (https://onlinelibrary.wiley.com/terms-and-conditions) on Wiley Online Library for rules of use; OA articles are governed by the applicable Creative Commons License

[38] S. Yakunin, M. Sytnyk, D. Kriegner, S. Shrestha, M. Richter, G. J. Matt, H. Azimi, C. J. Brabec, J. Stangl, M. V. Kovalenko, W. Heiss, *Nat. Photonics* **2015**, *9*, 444.
[39] K. Alkhalifah, A. Asbeutah, A. Brindhaban, *J. Clin. Imaging Sci.* **2020**, *10*, 56.
[40] J. H. Hubbell, S. M. Seltzer, *X-Ray Mass Attenuation Coefficients NIST Standard Reference Database 126*, Radiation Physics Division, PML, NIST, Gaithersburg **2004**.
[41] M. R. Kaçal, F. Akman, M. I. Sayyed, F. Akman, *Nucl. Eng. Technol.* **2019**, *51*, 818.
[42] J. A. Posar, J. Davis, O. Brace, P. Sellin, M. J. Griffith, O. Dhez, D. Wilkinson, M. L. F. Lerch, A. Rosenfeld, M. Petasecca, *Phys. Imaging Radiat. Oncol.* **2020**, *14*, 48.
[43] B. Fraboni, A. Fraleoni-Morgera, N. Zaitseva, *Adv. Funct. Mater.* **2015**, *26*, 2276.
[44] J. A. Davis, S. Guatelli, M. Petasecca, M. L. F. Lerch, M. I. Reinhard, M. Zaider, J. Ziegler, A. B. Rosenfeld, *IEEE Trans. Nucl. Sci.* **2014**, *61*, 1544.
[45] G. F. Knoll, *Radiation Detection and Measurement*, John Wiley, Hoboken, NJ **2010**.
[46] L. Basirico, I. Fratelli, M. Verdi, A. Ciavatti, L. Barba, O. Cesarini, G. Bais, M. Polentarutti, M. Chiari, B. Fraboni, *Adv. Sci.* **2022**, *10*, 2204815.
[47] I. Fratelli, A. Ciavatti, E. Zanazzi, L. Basirico, M. Chiari, L. Fabbri, J. E. Anthony, A. Quaranta, B. Fraboni, *Sci. Adv.* **2021**, *7*.
[48] S. Guatelli, D. Cutajar, B. Oborn, A. B. Rosenfeld, T. Kron, F. D'Errico, M. Moscovitch, *AIP Conf. Proc.* **2011**, *1345*, 303.
[49] K. Gill, G. Hall, B. MacEvoy, *J. Appl. Phys.* **1997**, *82*, 126.
[50] N. Keskitalo, P. Jonsson, K. Nordgren, H. Bleichner, E. Nordlander, *J. Appl. Phys.* **1998**, *83*, 4206.
[51] H. Wei, D. DeSantis, W. Wei, Y. Deng, D. Guo, T. J. Savenije, L. Cao, J. Huang, *Nat. Mater.* **2017**, *16*, 826.
[52] S. Morab, M. M. Sundaram, A. Pivrikas, *Coatings* **2023**, *13*, 1657.
[53] C. S. Jiang, M. Yang, Y. Zhou, B. To, S. U. Nanayakkara, J. M. Luther, W. Zhou, J. J. Berry, J. van de Lagemaat, N. P. Padture, K. Zhu, M. M. Al-Jassim, *Nat. Commun.* **2015**, *6*, 8397.
[54] J. Shi, Y. Li, Y. Li, D. Li, Y. Luo, H. Wu, Q. Meng, *Joule* **2018**, *2*, 879.
[55] S. Baranovski, *Charge transport in disordered solids with applications in electronics*, Wiley, Chichester, England **2006**.
[56] A. Köhler, H. Bässler, *Electronic Processes in Organic Semiconductors: An Introduction*, Wiley-VCH Verlag GmbH & Co, Weinheim, Germany **2015**.
[57] J. Wu, H. Cha, T. Du, Y. Dong, W. Xu, C. T. Lin, J. R. Durrant, *Adv. Mater.* **2022**, *34*, 2101833.
[58] O. Bubon, K. Jandieri, S. D. Baranovskii, S. O. Kasap, A. Reznik, *J. Appl. Phys.* **2016**, *119*, 124511.
[59] O. Grynko, T. Thibault, E. Pineau, A. Reznik, *Sensors* **2021**, *21*, 7321.
[60] P. Aguiar, J. Pardo-Montero, *Radiat. Phys. Chem.* **2016**, *119*, 173.
[61] I. Fratelli, L. Basiricò, A. Ciavatti, Z. A. Lamport, J. E. Anthony, I. Kymissis, B. Fraboni, *Adv. Mater. Technol.* **2022**, *8*, 2200769.
[62] L. Li, X. Liu, H. Zhang, B. Zhang, W. Jie, P. J. Sellin, C. Hu, G. Zeng, Y. Xu, *ACS Appl. Mater. Interfaces* **2019**, *11*, 7522.
[63] H. Wei, J. Huang, *Nat. Commun.* **2019**, *10*, 1066.
[64] A. Jana, S. Cho, S. A. Patil, A. Meena, Y. Jo, V. G. Sree, Y. Park, H. Kim, H. Im, R. A. Taylor, *Mater. Today* **2022**, *55*, 110.
[65] W. Pan, B. Yang, G. Niu, K. H. Xue, X. Du, L. Yin, M. Zhang, H. Wu, X. S. Miao, J. Tang, *Adv. Mater.* **2019**, *31*, 1904405.
[66] Y. Gao, Y. Ge, X. Wang, J. Liu, W. Liu, Y. Cao, K. Gu, Z. Guo, Y. M. Wei, N. Zhou, D. Yu, H. Meng, X. F. Yu, H. Zheng, W. Huang, J. Li, *Adv. Mater.* **2021**, *33*, 2101717.
[67] K. Liu, Y. Bian, J. Kuang, X. Huang, Y. Li, W. Shi, Z. Zhu, G. Liu, M. Qin, Z. Zhao, X. Li, Y. Guo, Y. Liu, *Adv. Mater.* **2022**, *34*, 2107304.
[68] J. Liu, B. Shabbir, C. Wang, T. Wan, Q. Ou, P. Yu, A. Tadich, X. Jiao, D. Chu, D. Qi, D. Li, R. Kan, Y. Huang, Y. Dong, J. Jasieniak, Y. Zhang, Q. Bao, *Adv. Mater.* **2019**, *31*, 1901644.
[69] L. Pan, Z. Liu, C. Welton, V. V. Klepov, J. A. Peters, M. C. De Siena, A. Benadia, I. Pandey, A. Miceli, D. Y. Chung, G. N. M. Reddy, B. W. Wessels, M. G. Kanatzidis, *Adv. Mater.* **2023**, *35*, 2211840.
[70] L. M. Herz, *ACS Energy Lett.* **2017**, *2*, 1539.
[71] Q. Chen, J. Wu, X. Ou, B. Huang, J. Almutlaq, A. A. Zhumekenov, X. Guan, S. Han, L. Liang, Z. Yi, J. Li, X. Xie, Y. Wang, Y. Li, D. Fan, D. B. L. Teh, A. H. All, O. F. Mohammed, O. M. Bakr, T. Wu, M. Bettinelli, H. Yang, W. Huang, X. Liu, *Nature* **2018**, *561*, 88.
[72] J. Zhao, L. Zhao, Y. Deng, X. Xiao, Z. Ni, S. Xu, J. Huang, *Nat. Photonics* **2020**, *14*, 612.
[73] S. Yakunin, D. N. Dirin, Y. Shynkarenko, V. Morad, I. Cherniukh, O. Nazarenko, D. Kreil, T. Nauser, M. V. Kovalenko, *Nat. Photonics* **2016**, *10*, 585.
[74] S. Demchyshyn, M. Verdi, L. Basirico, A. Ciavatti, B. Hailegnaw, D. Cavalcoli, M. C. Scharber, N. S. Sariciftci, M. Kaltenbrunner, B. Fraboni, *Adv. Sci.* **2020**, *7*, 2002586.
[75] G. Bizarri, *J. Crystal Growth* **2010**, *312*, 1213.
[76] T. Yanagida, *Proc. Jpn. Acad. B (Phys. Biol. Sci.)* **2018**, *94*, 75.
[77] B. Baramsai, B. M. Steinetz, L. Forsley, R. E. Martin, P. B. Ugorowski, M. D. Becks, T. L. Benyo, A. Chait, R. C. Hendricks, G. C. Fralick, N. Penney, M. Pines, C. E. Sandifer, *NASA Tech. Memo.* **2020**, TM20205008493.
[78] M. Cecconello, *J. Fusion Energy* **2019**, *38*, 356.
[79] M. Koshimizu, in *Phosphors for Radiation Detectors*, (Eds.: T. Yanagida, M. Koshimizu), John Wiley and Sons, New York **2022**.
[80] J. Wei, Y. Jiang, C. Liu, J. Duan, S. Liu, X. Liu, S. Liu, Y. Ma, Q. Zhao, *Adv. Photonics* **2022**, *4*, 035002.
[81] L. J. Xu, X. Lin, Q. He, M. Worku, B. Ma, *Nat. Commun.* **2020**, *11*, 4329.
[82] D. Anderson, S. Cottam, H. Heim, H. Zhang, N. P. Holmes, M. J. Griffith, *MRS Commun.* **2019**, *9*, 1206.
[83] X. Guan, W. Hu, M. A. Haque, N. Wei, Z. Liu, A. Chen, T. Wu, *Adv. Funct. Mater.* **2017**, *28*, 1704665.
[84] Y. He, M. Petryk, Z. Liu, D. G. Chica, I. Hadar, C. Leak, W. Ke, I. Spanopoulos, W. Lin, D. Y. Chung, B. W. Wessels, Z. He, M. G. Kanatzidis, *Nat. Photonics* **2020**, *15*, 36.
[85] M. Verdi, A. Ciavatti, J. Segura-Ruiz, L. Basiricò, R. Sorrentino, I. P. Goncalves, A. Petrozza, F. Boscherini, B. Fraboni, *Adv. Electron. Mater.* **2023**, *9*, 2201346.
[86] S. Morab, M. M. Sundaram, A. Pivrikas, *Materials* **2023**, *16*, 20230629.
[87] Y. Zhou, Y. Zhu, W. Xu, Q. Wang, *Adv. Energy Mater.* **2023**, *13*, 2203961.
[88] W. Pan, H. Wu, J. Luo, Z. Deng, C. Ge, C. Chen, X. Jiang, W.-J. Yin, G. Niu, L. Zhu, L. Yin, Y. Zhou, Q. Xie, X. Ke, M. Sui, J. Tang, *Nat. Photonics* **2017**, *11*, 726.
[89] R. Zhuang, X. Wang, W. Ma, Y. Wu, X. Chen, L. Tang, H. Zhu, J. Liu, L. Wu, W. Zhou, X. Liu, Y. Yang, *Nat. Photonics* **2019**, *13*, 602.
[90] N. Tamam, H. Salah, K. S. Almogren, O. Mahgoub, M. K. Saeed, Y. Abdullah, D. Thanh Tai, H. Omer, A. Sulieman, D. A. Bradley, *Radiat. Phys. Chem.* **2023**, *207*, 110818.
[91] A. Intaniwet, C. A. Mills, M. Shkunov, H. Thiem, J. L. Keddie, P. J. Sellin, *J. Appl. Phys.* **2009**, *106*, 1903.
[92] A. Intaniwet, J. L. Keddie, M. Shkunov, P. J. Sellin, *Org. Electron.* **2011**, *12*, 1903.
[93] A. Intaniwet, C. A. Mills, M. Shkunov, P. J. Sellin, J. L. Keddie, *Nanotechnology* **2012**, *23*, 235502.
[94] C. A. Mills, H. Al-Otaibi, A. Intaniwet, M. Shkunov, S. Pani, J. L. Keddie, P. J. Sellin, *J. Phys. D: Appl. Phys.* **2013**, *46*, 275102.
[95] H. Han, S. Lee, J. Seo, C. Mahata, S. H. Cho, A. R. Han, K. S. Hong, J. H. Park, M. J. Soh, C. Park, T. Lee, *Nanoscale Res. Lett.* **2014**, *9*, 2482.
[96] B. Fraboni, A. Ciavatti, F. Merlo, L. Pasquini, A. Cavallini, A. Quaranta, A. Bonfiglio, A. Fraleoni-Morgera, *Adv. Mater.* **2012**, *24*, 2289.

© 2025 The Author(s). Advanced Functional Materials published by Wiley-VCH GmbH

16163028, 2026, 21, Downloaded from https://advanced.onlinelibrary.wiley.com/doi/10.1002/adfm.202423521 by Adelaide University, Wiley Online Library on [30/09/2026]. See the Terms and Conditions (https://onlinelibrary.wiley.com/terms-and-conditions) on Wiley Online Library for rules of use; OA articles are governed by the applicable Creative Commons License

[97] B. Fraboni, A. Ciavatti, L. Basirico, A. Fraleoni-Morgera, *Faraday Discuss.* **2014**, *174*, 219.
[98] L. Basirico, A. Ciavatti, M. Sibilia, A. Fraleoni-Morgera, S. Trabattoni, A. Sassella, B. Fraboni, *IEEE Trans. Nucl. Sci.* **2015**, *62*, 1791.
[99] P. Büchele, M. Richter, S. F. Tedde, G. J. Matt, G. N. Ankah, R. Fischer, M. Biele, W. Metzger, S. Lilliu, O. Bikondoa, J. E. Macdonald, C. J. Brabec, T. Kraus, U. Lemmer, O. Schmidt, *Nat. Photonics* **2015**, *9*, 843.
[100] A. Ciavatti, E. Capria, A. Fraleoni-Morgera, G. Tromba, D. Dreossi, P. J. Sellin, P. Cosseddu, A. Bonfiglio, B. Fraboni, *Adv. Mater.* **2015**, *27*, 7213.
[101] L. Basirico, A. Ciavatti, T. Cramer, P. Cosseddu, A. Bonfiglio, B. Fraboni, *Nat. Commun.* **2016**, *7*, 13063.
[102] H. Wei, Y. Fang, P. Mulligan, W. Chuirazzi, H.-H. Fang, C. Wang, B. R. Ecker, Y. Gao, M. A. Loi, L. Cao, J. Huang, *Nat. Photonics* **2016**, *10*, 333.
[103] S. Lai, P. Cosseddu, L. Basiricò, A. Ciavatti, B. Fraboni, A. Bonfiglio, *Adv. Electron. Mater.* **2017**, *3*, 1600409.
[104] A. Ciavatti, T. Cramer, M. Carroli, L. Basiricò, R. Fuhrer, D. M. De Leeuw, B. Fraboni, *Appl. Phys. Lett.* **2017**, *111*, 183301.
[105] S. Shrestha, R. Fischer, G. J. Matt, P. Feldner, T. Michel, A. Osvet, I. Levchuk, B. Merle, S. Golkar, H. Chen, S. F. Tedde, O. Schmidt, R. Hock, M. Rührig, M. Göken, W. Heiss, G. Anton, C. J. Brabec, *Nat. Photonics* **2017**, *11*, 436.
[106] Y. C. Kim, K. H. Kim, D. Y. Son, D. N. Jeong, J. Y. Seo, Y. S. Choi, I. T. Han, S. Y. Lee, N. G. Park, *Nature* **2017**, *550*, 87.
[107] W. Wei, Y. Zhang, Q. Xu, H. Wei, Y. Fang, Q. Wang, Y. Deng, T. Li, A. Gruverman, L. Cao, J. Huang, *Nat. Photonics* **2017**, *11*, 315.
[108] A. Ciavatti, L. Basiricò, I. Fratelli, S. Lai, P. Cosseddu, A. Bonfiglio, J. E. Anthony, B. Fraboni, *Adv. Funct. Mater.* **2018**, *29*, 1806119.
[109] X. Wang, D. Zhao, Y. Qiu, Y. Huang, Y. Wu, G. Li, Q. Huang, Q. Khan, A. Nathan, W. Lei, J. Chen, *Physica Status Solidi RRL* **2018**, *12*.
[110] J. A. Steele, W. Pan, C. Martin, M. Keshavarz, E. Debroye, H. Yuan, S. Banerjee, E. Fron, D. Jonckheere, C. W. Kim, W. Baekelant, G. Niu, J. Tang, J. Vanacken, M. Van der Auweraer, J. Hofkens, M. B. J. Roeffaers, *Adv. Mater.* **2018**, *30*, 1804450.
[111] Y. Xu, B. Jiao, T.-B. Song, C. C. Stoumpos, Y. He, I. Hadar, W. Lin, W. Jie, M. G. Kanatzidis, *ACS Photonics* **2018**, *6*, 196.
[112] L. Basiricò, S. P. Senanayak, A. Ciavatti, M. Abdi-Jalebi, B. Fraboni, H. Sirringhaus, *Adv. Funct. Mater.* **2019**, *29*.
[113] F. Ye, H. Lin, H. Wu, L. Zhu, Z. Huang, D. Ouyang, G. Niu, W. C. H. Choy, *Adv. Funct. Mater.* **2019**, *29*, 1806984.
[114] M. Bruzzi, C. Talamonti, N. Calisi, S. Caporali, A. Vinattieri, *APL Mater.* **2019**, *7*.
[115] I. Temino, L. Basirico, I. Fratelli, A. Tamayo, A. Ciavatti, M. Mas-Torrent, B. Fraboni, *Nat. Commun.* **2020**, *11*, 2136.
[116] H. Tsai, F. Liu, S. Shrestha, K. Fernando, S. Tretiak, B. Scott, D. T. Vo, J. Strzalka, W. Nie, *Sci. Adv.* **2020**, *6*, aay0815.
[117] C. Ji, S. Wang, Y. Wang, H. Chen, L. Li, Z. Sun, Y. Sui, S. Wang, J. Luo, *Adv. Funct. Mater.* **2020**, *30*, 1905529.
[118] X. Zheng, W. Zhao, P. Wang, H. Tan, M. I. Saidaminov, S. Tie, L. Chen, Y. Peng, J. Long, W.-H. Zhang, *J. Energy Chem.* **2020**, *49*, 299.
[119] G. J. Matt, I. Levchuk, J. Knüttel, J. Dallmann, A. Osvet, M. Sytnyk, X. Tang, J. Elia, R. Hock, W. Heiss, C. J. Brabec, *Adv. Mater. Interfaces* **2020**, *7*.
[120] H. Zhang, G. Dun, Q. Feng, R. Zhao, R. Liang, Z. Gao, T. Hirtz, M. Chen, X. Geng, M. Liu, Y. Huang, X. Zheng, K. Qin, X. Tan, X. Wang, D. Xie, Y. Yang, H. Tian, Y. Zhou, N. P. Padture, X. Wang, J. Hong, T.-L. Ren, *IEEE Trans. Electron. Dev.* **2020**, *67*, 3191.
[121] M. Hu, S. Jia, Y. Liu, J. Cui, Y. Zhang, H. Su, S. Cao, L. Mo, D. Chu, G. Zhao, K. Zhao, Z. Yang, S. F. Liu, *ACS Appl. Mater. Interfaces* **2020**, *12*, 16592.
[122] Y. Song, L. Li, W. Bi, M. Hao, Y. Kang, A. Wang, Z. Wang, H. Li, X. Li, Y. Fang, D. Yang, Q. Dong, *Research* **2020**, *2020*, 5958243.
[123] X. Xu, W. Qian, J. Wang, J. Yang, J. Chen, S. Xiao, Y. Ge, S. Yang, *Adv. Sci.* **2021**, *8*, 2102730.
[124] A. Glushkova, P. Andricevic, R. Smajda, B. Nafradi, M. Kollar, V. Djokic, A. Arakcheeva, L. Forro, R. Pugin, E. Horvath, *ACS Nano* **2021**, *15*, 4077.
[125] Y. Liu, Y. Zhang, X. Zhu, J. Feng, I. Spanopoulos, W. Ke, Y. He, X. Ren, Z. Yang, F. Xiao, K. Zhao, M. Kanatzidis, S. F. Liu, *Adv. Mater.* **2021**, *33*, 2006010.
[126] Y. Song, L. Li, M. Hao, W. Bi, A. Wang, Y. Kang, H. Li, X. Li, Y. Fang, D. Yang, Q. Dong, *Adv. Mater.* **2021**, *33*, 2103078.
[127] L. Li, Y. Fang, D. Yang, *J. Phys. Chem. Lett.* **2022**, *13*, 5441.
[128] X. He, M. Xia, H. Wu, X. Du, Z. Song, S. Zhao, X. Chen, G. Niu, J. Tang, *Adv. Funct. Mater.* **2021**, *32*.
[129] J. Jiang, M. Xiong, K. Fan, C. Bao, D. Xin, Z. Pan, L. Fei, H. Huang, L. Zhou, K. Yao, X. Zheng, L. Shen, F. Gao, *Nat. Photonics* **2022**, *16*, 575.
[130] P. Zhang, Y. Hua, Y. Xu, Q. Sun, X. Li, F. Cui, L. Liu, Y. Bi, G. Zhang, X. Tao, *Adv. Mater.* **2022**, *34*, 2106562.
[131] J. Wu, L. Wang, A. Feng, S. Yang, N. Li, X. Jiang, N. Liu, S. Xie, X. Guo, Y. Fang, Z. Chen, D. Yang, X. Tao, *Adv. Funct. Mater.* **2022**, *32*, 2109149.
[132] A. Tamayo, I. Fratelli, A. Ciavatti, C. Martínez-Domingo, P. Branchini, E. Colantoni, S. De Rosa, L. Tortora, A. Contillo, R. Santiago, S. T. Bromley, B. Fraboni, M. Mas-Torrent, L. Basiricò, *Adv. Electron. Mater.* **2022**, *8*.
[133] M. Xu, M. Zhu, D. Zhao, S. Chen, S. Liu, Q. Zhang, P. Yuan, B. Zhang, P. Sellin, W. Jie, Y. Xu, *J. Mater. Sci. Technol.* **2023**, *135*, 46.
[134] B. Y. Li, M. J. Xie, J. Lu, W. F. Wang, R. Li, J. R. Mi, S. H. Wang, F. K. Zheng, G. C. Guo, *Small* **2023**, *19*, 2302492.
[135] P. Jin, Y. Tang, D. Li, Y. Wang, P. Ran, C. Zhou, Y. Yuan, W. Zhu, T. Liu, K. Liang, C. Kuang, X. Liu, B. Zhu, Y. M. Yang, *Nat. Commun.* **2023**, *14*, 626.
[136] Y. Song, L. Wang, Y. Shi, W. Bi, J. Chen, M. Hao, A. Wang, X. Yang, Y. Sun, F. Yu, L. Li, Y. Fang, D. Yang, Q. Dong, *Light Sci. Appl.* **2023**, *12*, 85.
[137] N. Li, Y. Li, S. Xie, J. Wu, N. Liu, Y. Yu, Q. Lin, Y. Liu, S. Yang, G. Lian, Y. Fang, D. Yang, Z. Chen, X. Tao, *Angew. Chem.* **2023**, *135*.
[138] K. Qin, G. H. Dun, Y. Y. Li, R. Zhao, X. Geng, J. H. Zhang, M. S. Zhang, R. L. Zhou, J. L. Peng, H. Tian, D. Xie, Y. Yang, T. L. Ren, *ACS Appl. Mater. Interfaces* **2023**, *15*, 37640.
[139] K. Guo, W. Li, Y. He, X. Feng, J. Song, W. Pan, W. Qu, B. Yang, H. Wei, *Angew. Chem.* **2023**, *135*.
[140] W. Huang, H. Chen, Z. Zhu, B. Zhao, S. Gao, Y. He, L. Yan, X. Wang, Y. Li, *Mater. Today Chem.* **2024**, *38*.
[141] X. Qin, J. Han, Y. Chai, B. Cao, A. Li, H. Zeng, X. Li, *ACS Appl. Mater. Interfaces* **2024**, *16*, 55705.
[142] X. Zhang, D. Chu, B. Jia, Z. Zhao, J. Pi, Z. Yang, Y. Li, J. Hao, R. Shi, X. Dong, Y. Liang, J. Feng, A. Najar, Y. Liu, S. F. Liu, *Adv. Mater.* **2024**, *36*, 2305513.
[143] L. Liu, M. Xu, X. Xu, X. Tao, Z. Gao, *Adv. Mater.* **2024**, *36*, 2406443.
[144] M. J. Griffith, K. Sunahara, A. Furube, A. J. Mozer, D. L. Officer, P. Wagner, G. G. Wallace, S. Mori, *J. Phys. Chem. C* **2013**, *117*, 11885.
[145] K. Sunahara, M. J. Griffith, T. Uchiyama, P. Wagner, D. L. Officer, G. G. Wallace, A. J. Mozer, S. Mori, *ACS Appl. Mater. Interfaces* **2013**, *5*, 10824.
[146] H. Mescher, F. Schackmar, H. Eggers, T. Abzieher, M. Zuber, E. Hamann, T. Baumbach, B. S. Richards, G. Hernandez-Sosa, U. W. Paetzold, U. Lemmer, *ACS Appl. Mater. Interfaces* **2020**, *12*, 15774.
[147] M. Z. Kabir, S. Kasap, in *Springer Handbook of Electronic and Photonic Materials*, (Eds.: S. Kasap, P. Capper), Springer International Publishing, Cham **2017**, p. 1.
[148] Y. He, I. Hadar, M. G. Kanatzidis, *Nat. Photonics* **2021**, *16*, 14.

© 2025 The Author(s). Advanced Functional Materials published by Wiley-VCH GmbH

16163028, 2026, 21, Downloaded from https://advanced.onlinelibrary.wiley.com/doi/10.1002/adfm.202423521 by Adelaide University, Wiley Online Library on [30/09/2026]. See the Terms and Conditions (https://onlinelibrary.wiley.com/terms-and-conditions) on Wiley Online Library for rules of use; OA articles are governed by the applicable Creative Commons License

[149] S. O. Kasap, *J. Phys. D: Appl. Phys.* **2000**, *33*, 2853.
[150] H. Toivonen, M. Dowdall, M. Baron, E. Kroeger, *Appl. Radiat. Isot.* **2023**, *198*, 110842.
[151] I. Szalóki, S. Szegedi, K. Varga, M. Braun, J. Osán, R. Van Grieken, *X-Ray Spectrom.* **2001**, *30*, 49.
[152] Y. Zhou, L. Zhao, Z. Ni, S. Xu, J. Zhao, X. Xiao, J. Huang, *Sci. Adv.* **2021**, *7*, abg6716.
[153] R. Kranzer, A. Schuller, A. Bourgouin, T. Hackel, D. Poppinga, M. Lapp, H. K. Looe, B. Poppe, *Phys. Med. Biol.* **2022**, *67*, 075002.
[154] E. Aboelezz, B. W. Pogue, *Appl. Phys. Rev.* **2023**, *10*, 021312.
[155] E. Grusell, G. Rikner, *Acta. Radiol. Oncol.* **1984**, *23*, 465.
[156] E. Grusell, G. Rikner, *Phys. Med. Biol.* **1993**, *38*, 785.
[157] R. A. Jagt, I. Bravic, L. Eyre, K. Galkowski, J. Borowiec, K. R. Dudipala, M. Baranowski, M. Dyksik, T. W. J. van de Goor, T. Kreouzis, M. Xiao, A. Bevan, P. Plochocka, S. D. Stranks, F. Deschler, B. Monserrat, J. L. MacManus-Driscoll, R. L. Z. Hoye, *Nat. Commun.* **2023**, *14*, 2452.
[158] Y. Li, W. Shao, L. Chen, J. Wang, J. Nie, H. Zhang, S. Zhang, R. Gao, X. Ouyang, X. Ouyang, Q. Xu, *NPG Asia Mater.* **2021**, *13*.
[159] W.-F. Wang, J. Lu, X.-M. Xu, B.-Y. Li, J. Gao, M.-J. Xie, S.-H. Wang, F.-K. Zheng, G.-C. Guo, *Chem. Eng. J.* **2022**, *430*.
[160] A. Ishikawa, K. Watanabe, A. Yamazaki, S. Yoshihashi, S. Imai, A. Masuda, T. Matsumoto, H. Tanaka, Y. Sakurai, M. Nogami, K. Hitomi, A. Uritani, H. Harano, *Nucl. Instrum. Methods A* **2022**, *1025*.
[161] G. Konstantatos, J. Clifford, L. Levina, E. H. Sargent, *Nat. Photonics* **2007**, *1*, 531.
[162] H. Beneking, *IEEE Trans. Electron. Dev.* **1982**, *29*, 1420.
[163] Y. Dan, X. Zhao, K. Chen, A. Mesli, *ACS Photonics* **2018**, *5*, 4111.
[164] D. Luo, X. Li, A. Dumont, H. Yu, Z. H. Lu, *Adv. Mater.* **2021**, *33*, 2006004.
[165] H. F. Haneef, A. M. Zeidell, O. D. Jurchescu, *J. Mater. Chem. C* **2020**, *8*, 759.
[166] S. Jia, Y. Xiao, M. Hu, X. He, N. Bu, N. Li, Y. Liu, Y. Zhang, J. Cui, X. Ren, K. Zhao, M. Liu, S. Wang, N. Yuan, J. Ding, Z. Yang, S. Liu, *Adv. Mater. Technol.* **2021**, *7*.
[167] K. Sakhatskyi, R. A. John, A. Guerrero, S. Tsarev, S. Sabisch, T. Das, G. J. Matt, S. Yakunin, I. Cherniukh, M. Kotyrba, Y. Berezovska, M. I. Bodnarchuk, S. Chakraborty, J. Bisquert, M. V. Kovalenko, *ACS Energy Lett.* **2022**, *7*, 3401.
[168] X. Xiao, J. Dai, Y. Fang, J. Zhao, X. Zheng, S. Tang, P. N. Rudd, X. C. Zeng, J. Huang, *ACS Energy Lett.* **2018**, *3*, 684.
[169] Y. Lin, Y. Bai, Y. Fang, Q. Wang, Y. Deng, J. Huang, *ACS Energy Lett.* **2017**, *2*, 1571.
[170] Y. Tu, Y. Xu, J. Li, Q. Hao, X. Liu, D. Qi, C. Bao, T. He, F. Gao, W. Zhang, *Small* **2020**, *16*, 2005626.
[171] J. G. Yukta, M. A. Afroz, S. Alghamdi, P. J. Sellin, S. Satapathi, *ACS Photonics* **2022**, *9*, 3529.
[172] F. Lédée, A. Ciavatti, M. Verdi, L. Basiricò, B. Fraboni, *Adv. Optic. Mater.* **2021**, *10*.
[173] B. Xiao, Q. Sun, F. Wang, S. Wang, B.-B. Zhang, J. Wang, W. Jie, P. Sellin, Y. Xu, *J. Mater. Chem. A* **2021**, *9*, 13209.
[174] M. P. A. Nanayakkara, M. G. Masteghin, L. Basirico, I. Fratelli, A. Ciavatti, R. C. Kilbride, S. Jenatsch, T. Webb, F. Richheimer, S. Wood, F. A. Castro, A. J. Parnell, B. Fraboni, K. Jayawardena, S. R. P. Silva, *Adv. Sci.* **2022**, *9*, 2101746.
[175] M. P. A. Nanayakkara, L. Matjačić, S. Wood, F. Richheimer, F. A. Castro, S. Jenatsch, S. Züfle, R. Kilbride, A. J. Parnell, M. G. Masteghin, H. M. Thirimanne, A. Nisbet, K. D. G. I. Jayawardena, S. R. P. Silva, *Adv. Funct. Mater.* **2020**, *31*.
[176] M. Asgari, H. Afarideh, H. Ghafoorifard, E. A Amirabadi, *Int. J. Rad. Res.* **2021**, *19*, 55.
[177] M.-J. Xie, J. Lu, B.-Y. Li, W.-F. Wang, S.-H. Wang, F.-K. Zheng, G.-C. Guo, *Chem. Eng. J.* **2023**, *466*, 143272.
[178] M. G. Barr, S. Chambon, A. Fahy, T. W. Jones, M. A. Marcus, A. L. D. Kilcoyne, P. C. Dastoor, M. J. Griffith, N. P. Holmes, *Mater. Chem. Front.* **2021**, *5*, 2218.
[179] A. J. Mozer, G. Dennler, N. S. Sariciftci, M. Westerling, A. Pivrikas, R. Österbacka, G. Juška, *Phys. Rev. B* **2005**, *72*.
[180] F. Akbari, E. I. Parsai, D. Shvydka, in *High-Z Materials for X-ray Detection*, (Eds.: L. Abbene, K. Iniewski), Springer, Cham **2023**.
[181] D. Kuciauskas, J. Moseley, P. Scajev, D. Albin, *Phys. Status Solidi-R* **2020**, *14*.
[182] O. G. Reid, M. Yang, N. Kopidakis, K. Zhu, G. Rumbles, *ACS Energy Lett.* **2016**, *1*, 561.
[183] C. Q. Xia, J. Peng, S. Ponce, J. B. Patel, A. D. Wright, T. W. Crothers, M. Uller Rothmann, J. Borchert, R. L. Milot, H. Kraus, Q. Lin, F. Giustino, L. M. Herz, M. B. Johnston, *J. Phys. Chem. Lett.* **2021**, *12*, 3607.
[184] T. M. Clarke, J. Peet, A. Nattestad, N. Drolet, G. Dennler, C. Lungenschmied, M. Leclerc, A. J. Mozer, *Org. Electron.* **2012**, *13*, 2639.
[185] G. Dennler, A. J. Mozer, G. Juška, A. Pivrikas, R. Österbacka, A. Fuchsbauer, N. S. Sariciftci, *Org. Electron.* **2006**, *7*, 229.
[186] W. D. Gill, *J. Appl. Phys.* **1972**, *43*, 5033.
[187] A. J. Mozer, N. S. Sariciftci, A. Pivrikas, R. Österbacka, G. Juška, L. Brassat, H. Bässler, *Phys. Rev. B* **2005**, *71*.
[188] J. A. Rohr, D. Moia, S. A. Haque, T. Kirchartz, J. Nelson, *J. Phys. Condens. Matter* **2018**, *30*, 105901.
[189] H. H. Choi, K. Cho, C. D. Frisbie, H. Sirringhaus, V. Podzorov, *Nat. Mater.* **2018**, *17*, 2.
[190] A. J. Campbell, R. Rawcliffe, A. Guite, J. C. D. Faria, A. Mukherjee, M. A. McLachlan, M. Shkunov, D. D. C. Bradley, *Adv. Funct. Mater.* **2016**, *26*, 3720.
[191] O. Baussens, L. Maturana, S. Amari, J. Zaccaro, J.-M. Verilhac, L. Hirsch, E. Gros-Daillon, *Appl. Phys. Lett.* **2020**, *117*.
[192] M. Martini, T. A. McMath, *Nucl. Instrum. Methods* **1970**, *79*, 259.
[193] Z. He, *Nucl. Instrum. Methods A* **2001**, *463*, 250.
[194] A. Zuck, M. Schieber, O. Khakhan, Z. Burshtein, *IEEE Trans. Nucl. Sci.* **2003**, *50*, 991.
[195] E. Vittone, *Nucl. Instrum. Methods B* **2004**, *219–220*, 1043.
[196] G. Juska, K. Arlauskas, M. Viliunas, J. Kocka, *Phys. Rev. Lett.* **2000**, *84*, 4946.
[197] A. J. Mozer, N. S. Sariciftci, L. Lutsen, D. Vanderzande, R. Österbacka, M. Westerling, G. Juška, *Appl. Phys. Lett.* **2005**, *86*.
[198] A. J. Mozer, C.-Q. Ma, W. W. H. Wong, D. J. Jones, P. Bäuerle, G. G. Wallace, *Org. Electron.* **2010**, *11*, 573.
[199] T. M. Clarke, C. Lungenschmied, J. Peet, N. Drolet, A. J. Mozer, *Adv. Energy Mater.* **2015**, *5*.
[200] B. Wright, Y. Nakajima, T. M. Clarke, K. Okuda, H. Paananen, A. J. Mozer, S. Mori, *Adv. Energy Mater.* **2017**, *7*.
[201] A. Baumann, J. Lorrmann, D. Rauh, C. Deibel, V. Dyakonov, *Adv. Mater.* **2012**, *24*, 4381.
[202] A. Armin, G. Juska, M. Ullah, M. Velusamy, P. L. Burn, P. Meredith, A. Pivrikas, *Adv. Energy Mater.* **2014**, *4*.
[203] S. Bange, M. Schubert, D. Neher, *Phys. Rev. B* **2010**, *81*.
[204] J. Lorrmann, B. H. Badada, O. Inganäs, V. Dyakonov, C. Deibel, *J. Appl. Phys.* **2010**, *108*.
[205] A. Armin, M. Velusamy, P. L. Burn, P. Meredith, A. Pivrikas, *Appl. Phys. Lett.* **2012**, *101*.
[206] M. Moll, E. Fretwurst, G. Lindström, *Nucl. Instrum. Methods A* **1999**, *426*, 87.
[207] M. J. Large, J. A. Posar, A. J. Mozer, A. Nattestad, S. Alnaghy, M. Carolan, P. J. Sellin, J. Davies, Z. Pastuovic, M. L. F. Lerch, S. Guatelli, A. Rosenfeld, M. J. Griffith, M. Petasecca, *ACS Appl. Mater. Interfaces* **2021**, *13*, 57703.

© 2025 The Author(s). Advanced Functional Materials published by Wiley-VCH GmbH

16163028, 2026, 21, Downloaded from https://advanced.onlinelibrary.wiley.com/doi/10.1002/adfm.202423521 by Adelaide University, Wiley Online Library on [30/09/2026]. See the Terms and Conditions (https://onlinelibrary.wiley.com/terms-and-conditions) on Wiley Online Library for rules of use; OA articles are governed by the applicable Creative Commons License

[208] J. A. Posar, C. Liao, L. Tegg, A. Ho-Baillie, M. Petasecca, M. J. Griffith, in *Metal-Halide Perovskite Semiconductors*, (Eds.: W. Nie, K. Iniewski), Springer, Cham., **2023**.
[209] J. A. Posar, M. J. Griffith, in *Advances in Fabrication and Investigation of Nanomaterials for Industrial Applications*, (Eds.: S. Krishnamoorthy, K. Iniewski), Springer, Cham, **2024**.
[210] T. Mizuno, T. Kamae, G. Godfrey, T. Handa, D. J. Thompson, D. Lauben, Y. Fukazawa, M. Ozaki, *Astrophys. J.* **2004**, *614*, 1113.
[211] S. Bartzsch, S. Corde, J. C. Crosbie, L. Day, M. Donzelli, M. Krisch, M. Lerch, P. Pellicioli, L. M. L. Smyth, M. Tehei, *Phys. Med. Biol.* **2020**, *65*, 02TR01.
[212] Z. Ahmed, L. T. Cumberland, N. N. Klimov, I. M. Pazos, R. E. Tosh, R. Fitzgerald, *Sci. Rep.* **2018**, *8*, 13007.
[213] A. Šagátová, B. Zaťko, F. Dubecký, T. Ly Anh, V. Nečas, K. Sedlačková, M. Pavlovič, M. Fülöp, *Appl. Surf. Sci.* **2017**, *395*, 66.
[214] D. M. Fleetwood, H. A. Eisen, *IEEE Trans. Nucl. Sci.* **2003**, *50*, 552.
[215] M. Ishii, K. Harada, Y. Hirose, N. Senguttuvan, M. Kobayashi, I. Yamaga, H. Ueno, K. Miwa, F. Shiji, F. Yiting, M. Nikl, X. Q. Feng, *Opt. Mater.* **2002**, *19*, 201.
[216] E. R. Benton, E. V. Benton, *Nucl. Instrum. Methods Phys. Res. B* **2001**, *184*, 255.
[217] E. E. Klein, J. Hanley, J. Bayouth, F. F. Yin, W. Simon, S. Dresser, C. Serago, F. Aguirre, L. Ma, B. Arjomandy, C. Liu, C. Sandin, T. Holmes, *Med. Phys.* **2009**, *36*, 4197.
[218] A. Kumar, R. Devine, C. Mayberry, B. Lei, G. Li, Y. Yang, *Adv. Funct. Mater.* **2010**, *20*, 2729.
[219] R. A. Street, J. E. Northrup, B. S. Krusor, *Phys. Rev. B* **2012**, *85*, 205211.
[220] S. Yang, Z. Xu, S. Xue, P. Kandlakunta, L. Cao, J. Huang, *Adv. Mater.* **2019**, *31*, 1805547.
[221] Q. Xu, H. Zhang, J. Nie, W. Shao, X. Wang, B. Zhang, X. Ouyang, *Radiat. Phys. Chem.* **2021**, *181*, 109337.
[222] T. Agostinelli, M. Campoy-Quiles, J. C. Blakesley, R. Speller, D. D. C. Bradley, J. Nelson, *Appl. Phys. Lett.* **2008**, *93*, 203305.
[223] J. C. Blakesley, P. E. Keivanidis, M. Campoy-Quiles, C. R. Newman, Y. Jin, R. Speller, H. Sirringhaus, N. C. Greenham, J. Nelson, P. Stavrinou, *Nucl. Instrum. Methods A* **2007**, *580*, 774.
[224] P. E. Keivanidis, N. C. Greenham, H. Sirringhaus, R. H. Friend, J. C. Blakesley, R. Speller, M. Campoy-Quiles, T. Agostinelli, D. D. C. Bradley, J. Nelson, *Appl. Phys. Lett.* **2008**, *92*.
[225] X. Dai, C. Fei, P. Kandlakunta, L. Zhao, Z. Ni, L. R. Cao, J. Huang, *IEEE Trans. Nucl. Sci.* **2022**, *69*, 1850.
[226] A. G. Boldyreva, A. F. Akbulatov, S. A. Tsarev, S. Y. Luchkin, I. S. Zhidkov, E. Z. Kurmaev, K. J. Stevenson, V. G. Petrov, P. A. Troshin, *J. Phys. Chem. Lett.* **2019**, *10*, 813.
[227] J. A. Posar, M. Large, S. Alnaghy, J. R. Paino, D. J. Butler, M. J. Griffith, S. Hood, M. L. F. Lerch, A. Rosenfeld, P. J. Sellin, S. Guatelli, M. Petasecca, *J. Synchrotron Radiat.* **2021**, *28*, 1444.
[228] A. Bashiri, M. J. Large, M. J. Griffith, L. Papale, B. Philippa, C. Hall, D. Bolst, S. Guatelli, A. J. Mozer, M. Petasecca, J. A. Posar, *Adv. Funct. Mater.* **2025**, *35*, 2415723.
[229] A. R. Kirmani, T. A. Byers, Z. Ni, K. VanSant, D. K. Saini, R. Scheidt, X. Zheng, T. B. Kum, I. R. Sellers, L. McMillon-Brown, J. Huang, B. Rout, J. M. Luther, *Nat. Commun.* **2024**, *15*, 696.
[230] G. Li, Y. Yang, R. A. Devine, C. Mayberry, *Nanotechnology* **2008**, *19*, 424014.
[231] L. Pernigoni, U. Lafont, A. M. Grande, *CEAS Space J.* **2021**, *13*, 341.
[232] M. Daum, S. Deumel, M. Sytnyk, H. A. Afify, R. Hock, A. Eigen, B. Zhao, M. Halik, A. These, G. J. Matt, C. J. Brabec, S. F. Tedde, W. Heiss, *Adv. Funct. Mater.* **2021**, *31*, 2102713.
[233] C. Xiao, Z. Li, H. Guthrey, J. Moseley, Y. Yang, S. Wozny, H. Moutinho, B. To, J. J. Berry, B. Gorman, Y. Yan, K. Zhu, M. Al-Jassim, *J. Phys. Chem. C* **2015**, *119*, 26904.
[234] L. L. Chua, M. Dipankar, S. Sivaramakrishnan, X. Gao, D. Qi, A. T. Wee, P. K. Ho, *Langmuir* **2006**, *22*, 8587.
[235] K. Yoshino, S. Hayashi, G. Ishii, Y. Inuishi, *Solid State Commun.* **1983**, *46*, 405.
[236] A. Erroi, S. Mecca, M. L. Zaffalon, I. Frank, F. Carulli, A. Cemmi, I. Di Sarcina, D. Debellis, F. Rossi, F. Cova, K. Pauwels, M. Mauri, J. Perego, V. Pinchetti, A. Comotti, F. Meinardi, A. Vedda, E. Auffray, L. Beverina, S. Brovelli, *ACS Energy Lett.* **2023**, *8*, 3883.
[237] J. W. Kingsley, S. J. Weston, D. G. Lidzey, *IEEE J. Selected Topics Quant. Electron.* **2010**, *16*, 1770.
[238] Y. Miyazawa, M. Ikegami, T. Miyasaka, T. Ohshima, M. Imaizumi, K. Hirose, Proc. IEEE 42nd Photovoltaics Specialist Conference (PVSC), New Orleans, USA **2015**, pp. 1–4.
[239] J.-S. Huang, M. D. Kelzenberg, P. Espinet-González, C. Mann, D. Walker, A. Naqavi, N. Vaidya, E. Warmann, H. A. Atwater, Proc. IEEE 44th Photovoltaics Specialist Conference (PVSC) **2017**, Washington, USA, pp. 1248–1252.
[240] Y. Miyazawa, M. Ikegami, H. W. Chen, T. Ohshima, M. Imaizumi, K. Hirose, T. Miyasaka, *iScience* **2018**, *2*, 148.
[241] J. Ran, O. Dyck, X. Wang, B. Yang, D. B. Geohegan, K. Xiao, *Adv. Energy Mater.* **2020**, *10*, 1903191.
[242] S. Diebold, P. Azzarello, E. Del Monte, M. Feroci, J. Jochum, E. Kendziorra, E. Perinati, A. Rachevski, A. Santangelo, C. Tenzer, A. Vacchi, G. Zampa, N. Zampa, *Nucl. Instrum. Methods A* **2013**, *721*, 65.
[243] F. Tommasino, M. Rovituso, S. Fabiano, S. Piffer, C. Manea, S. Lorentini, S. Lanzone, Z. Wang, M. Pasini, W. J. Burger, C. La Tessa, E. Scifoni, M. Schwarz, M. Durante, *Nucl. Instrum. Methods A* **2017**, *869*, 15.
[244] Y. Zhang, Y. Tu, X. Yang, R. Su, W. Yang, M. Yu, Y. Wang, W. Huang, Q. Gong, R. Zhu, *ACS Appl. Mater. Interfaces* **2020**, *12*, 24905.
[245] E. Sengbusch, A. Perez-Andujar, P. M. DeLuca, Jr., T. R. Mackie, *Med. Phys.* **2009**, *36*, 364.
[246] M. H. Du, *J. Mater. Chem. A* **2014**, *2*, 9091.
[247] F. Lang, N. H. Nickel, J. Bundesmann, S. Seidel, A. Denker, S. Albrecht, V. V. Brus, J. Rappich, B. Rech, G. Landi, H. C. Neitzert, *Adv. Mater.* **2016**, *28*, 8726.
[248] N. Yoshizawa, O. Sato, S. Takagi, S. Furihata, J. Funabiki, S. Iwai, T. Uehara, S.-i. Tanaka, Y. Sakamoto, *J. Nuclear Sci. Technol.* **2014**, *37*, 865.
[249] R. Mohan, *Precis. Radiat. Oncol.* **2022**, *6*, 164.
[250] D. G. Darambara, *Nucl. Instrum. Methods A* **2006**, *569*, 153.
[251] T. F. Sanquist, P. Doctor, R. Parasuraman, *IEEE Trans. Sys., Man, and Cybernetics, Part C (Appl. Rev.)* **2008**, *38*, 856.
[252] E. Lysenko, A. Rogachev, O. Starý, *Recent Developments in the Field of Non-Destructive Testing, Safety and Materials Science*, Springer, Cham **2022**.
[253] J. T. Bushberg, J. A. Seibert, E. M. L. Jr, J. M. Boone, *The Essential Physics of Medical Imaging*, Lippincott Williams & Wilkins, USA **2012**.
[254] J. L. Prince, J. M. Links, *Medical Imaging Signals and Systems*, Pearson Prentice Hall, USA **2006**.
[255] H. E. Martz, C. M. Logan, D. J. Schneberk, P. J. Shull, *X-Ray Imaging: Fundamentals, Industrial Techniques and Applications, Taylor and Frances*, CRC Press, Florida, USA **2017**.
[256] H. Wu, Y. Ge, G. Niu, J. Tang, *Matter* **2021**, *4*, 144.
[257] A. Tompe, K. Sargar, *X-Ray Image Quality Assurance*, National Library of Medicine (StatPearls Publishing), Florida **2025**,
[258] E. Samei, M. J. Flynn, D. A. Reimann, *Med. Phys.* **1998**, *25*, 102.
[259] Y. Zhou, J. Chen, O. M. Bakr, O. F. Mohammed, *ACS Energy Lett.* **2021**, *6*, 739.
[260] U. Neitzel, S. Gunther-Kohfahl, G. Borasi, E. Samei, *Med. Phys.* **2004**, *31*, 2205.
[261] I. Cunningham, in *Handbook of Medical Imaging*, Vol. *1*, Physics and Psychophysics, New York **2000**, pp. 79–159.

© 2025 The Author(s). Advanced Functional Materials published by Wiley-VCH GmbH

16163028, 2026, 21, Downloaded from https://advanced.onlinelibrary.wiley.com/doi/10.1002/adfm.202423521 by Adelaide University, Wiley Online Library on [30/09/2026]. See the Terms and Conditions (https://onlinelibrary.wiley.com/terms-and-conditions) on Wiley Online Library for rules of use; OA articles are governed by the applicable Creative Commons License



Jessie A. Posar received a Ph.D. in Physics from the University of Wollongong, Australia. She completed a postdoctoral research appointment at the University of Sydney in 2022 before being awarded a National Intelligence Postdoctoral Research Fellowship from the Office of National Intelligence and joining the Faculty of Engineering at the University of Wollongong in 2023. Her research focuses on the development of novel printable materials for radiation detection.



Matthew J. Griffith received a Ph.D. in Chemistry from the University of Wollongong in 2012. He has worked as a NEDO Fellow at Shinshu University in Japan, before returning to Australia and holding appointments as a post-doc and then Lecturer in Physics at the University of Newcastle (2013–2019), a Research Manager at the University of Sydney (2020–2023) and currently, an Associate Professor and ARC Future Fellow at the University of South Australia, where he leads the Centre for Nanoelectronic Devices. His research focuses on developing soft electroactive materials for applications in energy, bioelectronics, and applied physics.

© 2025 The Author(s). Advanced Functional Materials published by Wiley-VCH GmbH

16163028, 2026, 21, Downloaded from https://advanced.onlinelibrary.wiley.com/doi/10.1002/adfm.202423521 by Adelaide University, Wiley Online Library on [30/09/2026]. See the Terms and Conditions (https://onlinelibrary.wiley.com/terms-and-conditions) on Wiley Online Library for rules of use; OA articles are governed by the applicable Creative Commons License